

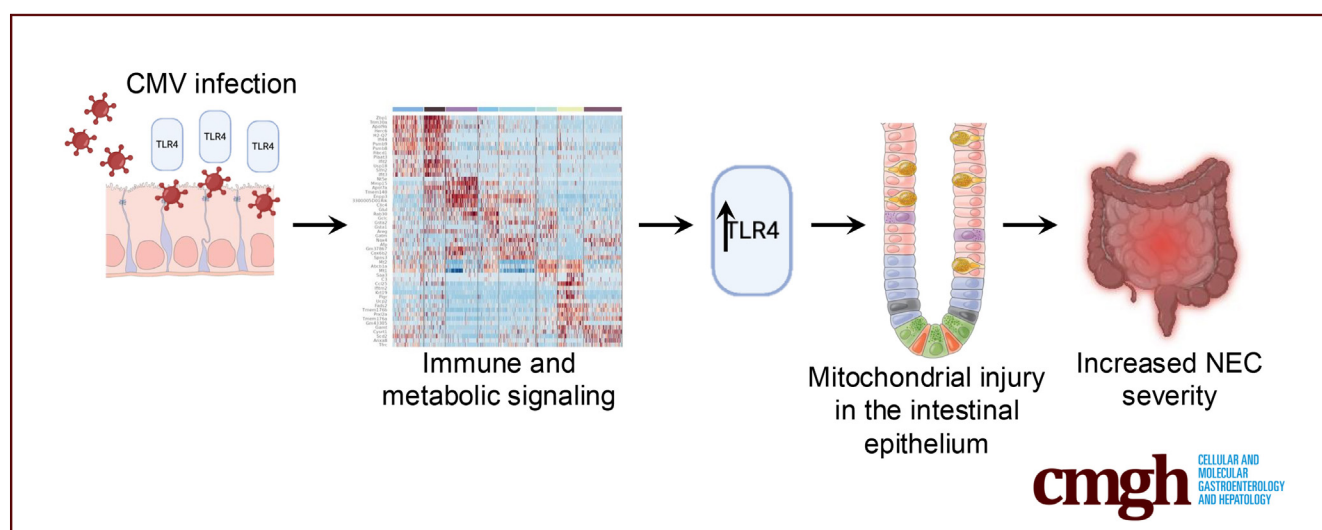
## ORIGINAL RESEARCH

## Cytomegalovirus Worsens Necrotizing Enterocolitis Severity in Mice via Increased Toll-Like Receptor 4 Signaling



Daniel Scheese, Peng Lu, Hannah Moore, Koichi Tsuboi, Cody Tragesser, Johannes Dues, Zachariah Raouf, Maame F. Sampah, Daphne Klerk, Mahmoud El Baassiri, Hee-seong Jang, Sierra Williams-McLeod, Asuka Ishiyama, Steve N. Steinway, Sanxia Wang, Menghan Wang, Thomas Prindle Jr., William B. Fulton, Chhinder P. Sodhi, and David J. Hackam

Division of Pediatric Surgery, Johns Hopkins University School of Medicine, and the Johns Hopkins Children's Center, Baltimore, Maryland



## SUMMARY

Cytomegalovirus infection worsens necrotizing enterocolitis severity by increasing toll-like receptor 4 signaling and causing mitochondrial dysfunction. Administration of a receptor agonist attenuates necrotizing enterocolitis by reducing the deleterious effects of cytomegalovirus on mitochondrial function and by reversing the effects of cytomegalovirus on toll-like receptor 4 signaling within the intestinal mucosa.

**BACKGROUND AND AIMS:** Necrotizing enterocolitis (NEC) is a life-threatening condition in premature infants, marked by acute intestinal necrosis. NEC develops in part after activation of the lipopolysaccharide receptor toll-like receptor 4 (TLR4) by intestinal microbes in the intestinal epithelium. Previous authors have shown an increased risk of NEC in human infants after cytomegalovirus (CMV) infection, which can affect mitochondrial function. We now seek to explore the impact and the mechanisms of CMV infection on NEC severity and its relationship with TLR4 signaling and mitochondria function.

**METHODS:** NEC was induced in newborn mice with and without CMV infection. RNA sequencing and gene set

enrichment analysis were performed to identify effects on inflammatory and metabolic pathways. The role of TLR4 signaling and mitochondrial function were investigated in wild-type and *Tlr4*-deficient mice. The adenosine receptor agonist 5'-N-ethylcarboxamido adenosine was tested for its ability to reduce CMV-induced effects on NEC severity.

**RESULTS:** CMV infection significantly increased NEC severity in wild-type mice. Mechanistically, CMV infection triggered proinflammatory pathways, disrupted cellular metabolism, and upregulated *Tlr4* expression, leading to mitochondrial dysfunction and nuclear factor- $\kappa$ B translocation. These effects were notably absent in *Tlr4*-deficient mice. 5'-N-ethylcarboxamido adenosine treatment reversed CMV-induced NEC severity by reducing mitochondrial dysfunction and TLR4-driven nuclear factor- $\kappa$ B activation.

**CONCLUSIONS:** CMV infection worsens NEC severity in mice by amplifying TLR4 signaling, inflammation, and mitochondrial dysfunction. Targeting CMV and its influence on TLR4 may offer novel therapeutic approaches for NEC. (*Cell Mol Gastroenterol Hepatol* 2025;19:101473; <https://doi.org/10.1016/j.jcmgh.2025.101473>)

**Keywords:** Necrotizing Enterocolitis; Cytomegalovirus; TLR4 Signaling.

This article has an accompanying editorial.

**N**ecrotizing enterocolitis (NEC) is a devastating disease of premature infants characterized by rapid intestinal necrosis, leading to death in nearly a third of affected patients.<sup>1,2</sup> Up to 10% of premature infants develop NEC,<sup>3</sup> and unfortunately, the survival rate of patients with NEC has remained unchanged over the past 3 decades.<sup>4</sup> These sobering statistics highlight the need for greater insights into disease pathogenesis and new therapeutic approaches.

Current thinking suggests that NEC develops from an excessive inflammatory response within the immature intestinal mucosa.<sup>5</sup> This proinflammatory state is partly caused by persistently elevated expression of the lipopolysaccharide (LPS) receptor toll-like receptor 4 (TLR4) in the premature infant,<sup>6</sup> which becomes activated by an abnormal intraluminal accumulation of bacteria of the *Enterobacteriaceae* family.<sup>7</sup> TLR4 activation damages the intestinal epithelium through a combination of apoptosis<sup>8,9</sup> and necroptosis,<sup>10</sup> and impairs mucosal repair by reducing enterocyte proliferation and migration.<sup>11,12</sup> Importantly, the factors leading to elevated TLR4 activation in the premature gut remain largely undefined, which may explain variations in NEC severity among patients with similar risk factors of prematurity and formula feeds.<sup>13</sup>

In seeking to identify the potential role for unexplored risk factors for NEC severity, we now explore the potential role for cytomegalovirus (CMV) infection. CMV is a herpesvirus with a global seroprevalence ranging from 40% to 80%.<sup>14</sup> CMV infection is generally asymptomatic in healthy individuals, but poses significant risks to the fetus during pregnancy, leading to congenital anomalies that are thought to be related in part to mitochondrial dysfunction.<sup>15–19</sup> Based on these findings, we now hypothesize that CMV infection contributes to NEC severity by enhancing intestinal TLR4 signaling and inducing mitochondrial dysfunction. We now show that CMV infection increases NEC severity in neonatal mouse models, and that administration of the adenosine receptor agonist 5'-N-ethylcarboxamido adenosine (NECA) can reverse these effects, offering a potential new therapy for this devastating disease.

## Results


### Murine CMV Infection Increases the Severity of NEC in Neonatal Mice

To determine whether murine CMV (mCMV) infection contributes to the severity of NEC, we developed a model of perinatal mCMV infection in mice (Figure 1A). Development of such a model is challenging, because simple delivery of mCMV to pregnant dams results in rapid viral clearance.<sup>20</sup> To overcome this clearance effect, we explored alternative approaches that bypass the dam, and therefore administered mCMV

directly into the pup, in utero and immediately postnatally ( $\leq 12$ –18 hours after birth), to mimic potential routes of human neonatal CMV transmission. Specifically, we tested mCMV delivery in utero using ultrasound-guided intrachorionic villi injection or ultrasound-guided injection into the amniotic fluid, and postnatal injection of pups within 12–24 hours after birth. mCMV infection in the ileum was determined by the expression of early antigen (*Ie1*) and interferon-gamma (*Ifng*), 2 genes that are known to be increased in response to mCMV infection.<sup>21–23</sup> Compared with mice in which mCMV was administered directly to the pregnant dam by intraperitoneal injection in which neither *Ie1* nor *Ifng* were upregulated in the fetuses (Figure 1B and C), the expression of both *Ie1* and *Ifng* were increased in the intestinal mucosa of pups in which mCMV was delivered into the placenta (Figure 1D and E), to the amniotic fluid (Figure 1F and G) or directly to the pups within 12–18 hours after birth (Figure 1H and I). Because in utero delivery of mCMV injection resulted in significant fetal loss caused by the trauma of injection, we adopted Model 4 in which mCMV was directly injected into neonatal pups for the subsequent studies, which allowed for further studies on the role of CMV in NEC pathogenesis.

mCMV was detected in the ileal tissues of newborn pups at 7 and 12 days postinjection, as revealed by the expression of *Ie1* by quantitative reverse transcription polymerase chain reaction (qRT-PCR) (Figure 1J). Interestingly, the virus seemed to be cleared by 28 days, because *Ie1* was no longer detectable by qRT-PCR at that time point. After confirming CMV infection via qRT-PCR (Figure 2A) and immunostaining in infected but not in uninfected mice (Figure 2B and C), the pups were then subjected to an established NEC model that was comprised of the administration of infant formula feeds, intermittent hypoxia, and gavage with bacteria from the stool of an infant with severe NEC, in the presence or absence of mCMV infection. Importantly, mCMV infection resulted in significantly increased NEC severity, as revealed by increased mucosal injury to the small intestine (Figure 2D and E), increased expression of 3'-nitrotyrosine (3'-NT) (Figure 2F–J), increased staining for dihydroethidium (DHE) (Figure 2K–O), increased expression of the proinflammatory cytokines *Ifng* (Figure 2P) and tumor necrosis factor (*Tnf*) (Figure 2Q), and increased detection of mitochondrial DNA (mtDNA) nicks (Figure 2R) in the ilea of

**Abbreviations:** 3'-NT, 3'-nitrotyrosine; ATCC, American Type Culture Collection; ATP, adenosine triphosphate; CMV, cytomegalovirus; DHE, dihydroethidium; GSEA, gene set enrichment analysis; H&E, hematoxylin-eosin; IEC-6, intestinal epithelial cells; *Ifng*, interferon gamma; LPS, lipopolysaccharide; mCMV, murine cytomegalovirus; mtDNA, mitochondrial DNA; NEC, necrotizing enterocolitis; NECA, 5'-N-ethylcarboxamido adenosine; NF- $\kappa$ B, nuclear factor kappa B; qRT-PCR, quantitative reverse transcription polymerase chain reaction; ROS, reactive oxygen species; scRNA-seq, single-cell RNA sequencing; TLR4, toll-like receptor 4; *Tnf*, tumor necrosis factor.

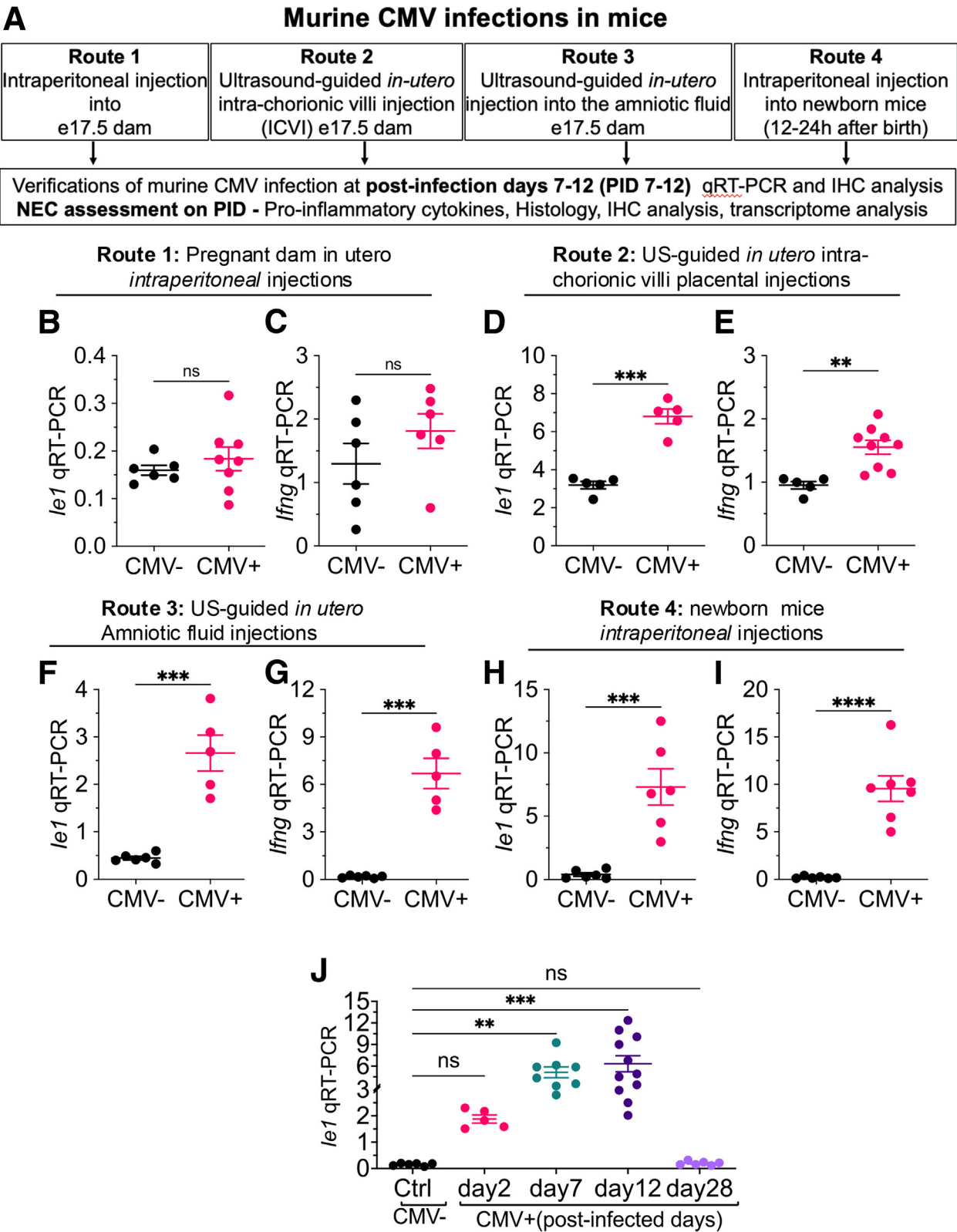
 Most current article

© 2025 The Authors. Published by Elsevier Inc. on behalf of the AGA Institute. This is an open access article under the CC BY-NC-ND license (<http://creativecommons.org/licenses/by-nc-nd/4.0/>).

2352-345X

<https://doi.org/10.1016/j.jcmgh.2025.101473>

mCMV infected mice with NEC as compared with uninfected mice and control animals without NEC. In parallel experiments, breastfed mice that were not exposed to the NEC model but which were infected with mCMV as above showed a significant increase in DHE, *Ifng*, *Tnf*, and mtDNA nicks above baseline, indicating that mCMV infection alone





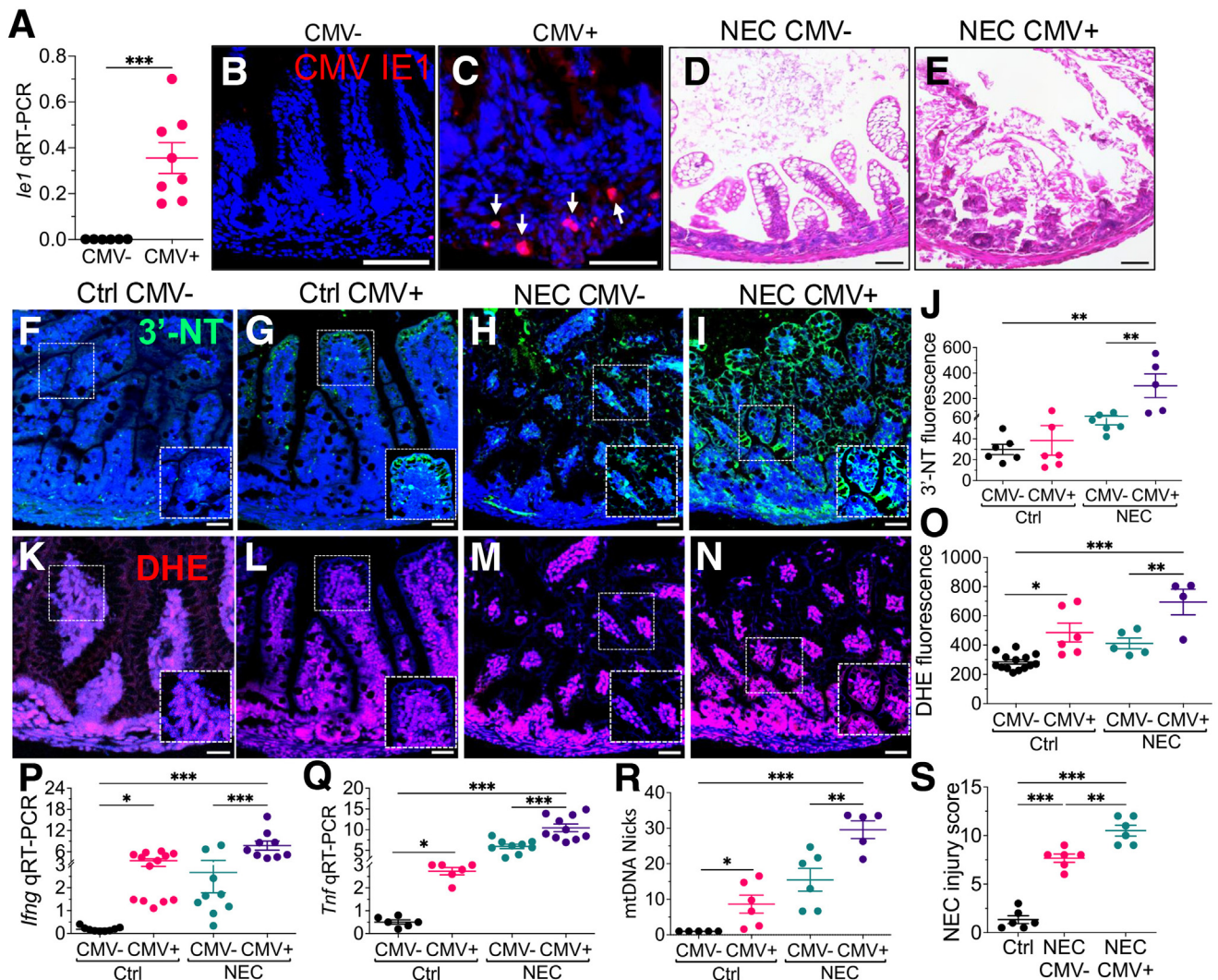


**Figure 2. Murine CMV infection increases NEC severity in neonatal mice.** (A) Expression by qRT-PCR of murine CMV antigen *le1* in ilea of neonatal mice in presence or absence of CMV infection. (B, C) Representative confocal images of neonatal mouse small bowel sections stained with anti-CMV immediate early antigen, IE1 (IE1 red, white arrows; DAPI blue). Representative H&E stained distal ileal sections in CMV<sup>-</sup> NEC (D) and CMV<sup>+</sup> NEC (E) mice. (F-I, K-N) Representative confocal images of ileal sections stained with the oxidative-injury marker, 3-nitrotyrosine (green, 3'-NT; blue, DAPI F-I) and ROS marker DHE (red, DHE; blue, DAPI; K-N). (J, O) Quantification of fluorescent intensity. Expression by qRT-PCR of *IFNG* (P) and *TNF* (Q). (R) Mitochondrial damage, calculated as nicks/16kb mouse mitochondrial genome. (S) Total injury score in the indicated group, as defined in Methods. Statistical significance was determined by 1-way analysis of variance followed by Tukey's multiple comparisons tests or unpaired t-test using GraphPad Prism 10 software. \**P* < .05, \*\**P* < .01, \*\*\**P* < .001. Scale bars, 50 μm. Data from 6–10 mice per group.

can induce an inflammatory response in the intestinal mucosa (Figure 2F-R). Consistent with these findings, mCMV-infected mice that were subjected to the NEC model

exhibited significantly higher NEC injury scores (as defined in Methods), compared with uninfected NEC mice (Figure 2S). As shown in Figure 2S, mCMV infection in

**Figure 1. (See previous page). Development of experimental models of perinatal murine CMV infection routes in mice.** (A) Schematic depicting the 4 routes of experimental murine CMV infection as described in Methods. (B, C) Route 1: intraperitoneal injections, in C57Bl/6 pregnant dams at embryonic day 17.5 (e17.5). (D, E) Route 2: Ultrasound (US)-guided in utero injection into the placenta (intrachorionic villi injection). (F, G) Route 3: US-guided in utero injection into the amniotic fluid. (H, I) Route 4: intraperitoneal injections in newborn mice within 12–24 hours after birth, showing qRT-PCR of murine CMV immediate early gene (*le1*) (B, D, F, H) and *Ifng* (C, E, G, I), in the ileal tissue mice of CMV-injected mice. (J) Murine CMV infection in newborn mice persists until postinfection day 12, as revealed by qRT-PCR of murine CMV immediate early gene (*le1*) in the ileal tissue on the indicated day after infection, infected at birth with murine CMV. Statistical significance was determined by 1-way analysis of variance followed by Tukey's multiple comparisons tests or unpaired t-test using GraphPad Prism 10 software. \*\**P* < .01, \*\*\**P* < .001, \*\*\*\**P* < .0001, ns, nonsignificant (*P* > .5), each dot is data from a different mouse (n = ≥5 mice/group).



breastfed mice did not independently induce NEC. These findings suggest that although mCMV increases the severity of NEC, it is insufficient to cause NEC on its own. We next sought to investigate the mechanisms by which CMV infection increases NEC severity in mice.

### *Patterns of Gene Expression in the Intestinal Epithelium of CMV-Infected Mice*

We next used single-cell RNA sequencing (scRNA-seq) to determine whether murine-CMV infection could induce cell-specific phenotypic alterations in the intestines of mice and thus contribute to the development of NEC. To do so, a scRNA-seq dataset was generated by integrating 4 replicates from the 4 different treatment groups (ie, breastfed control, perinatal mCMV infection without NEC, NEC without mCMV, and NEC with perinatal mCMV infection). After quality control, dimensional reduction, and Uniform Manifold Approximation and Projection, we used both marker genes and correlations to published scRNA-seq databases to identify the cellular populations within 20 clusters (Figure 3A). Of these 20 clusters, 8 were enterocyte sub-clusters, which on further analysis were revealed to separate into distinct enterocyte subtypes based on the presence of mCMV infection and NEC (Figure 3B and C). We examined the proportions of each cell type by condition and found that enterocyte clusters 4 and 5 were primarily from the unperturbed control samples. Enterocyte clusters 1, 2, and 3 were primarily from NEC samples, and enterocyte clusters 6 and 7 were primarily found in the mCMV samples (Figure 3D). The NEC+CMV group's cell proportions matched up most similarly to NEC but did have some increase in enterocyte 7, similar to mCMV-alone samples (Figure 3D). This scRNA-seq analysis revealed a phenotypic transformation in enterocyte cells caused by murine-CMV infection, which was explored further by isolating enterocyte clusters and performing gene set enrichment analysis (GSEA). This analysis, visualized with a network plot, determined that CMV infection leads to an upregulation in immune pathways and a decrease in pathways linked to cellular metabolism (Figure 4A). To examine in more detail these genes of interest, we generated stacked violin plots, which allowed us to visualize expression changes in these genes between CMV-infected and control subjects, and then validated the expression of each of the genes whose expression was significantly increased or decreased (Figure 4B and C) by qRT-PCR (Figure 4D-K). Based on the Kyoto Encyclopedia of Genes and Genomes pathway analysis, we identified that perinatal mCMV infection altered key genes that were linked to TLR4 signaling (Figure 4D-G), viral-related genes (Figure 4H and I), and mitochondrial energy metabolism (Figure 4J and K). For completeness, we also show how perinatal mCMV infection in mice altered the transcriptome of a variety of key metabolic genes within the small intestine as evidenced by the validation of multiple genes by qRT-PCR (Figure 5). In light of the GSEA findings shown in Figure 4 and the critical role for TLR4 signaling in NEC,<sup>24</sup> we next focused our investigations on understanding the effects of mCMV infection on TLR4 signaling.

### *Murine CMV Infection in Newborn Mice Leads to Increased TLR4 Signaling in the Intestinal Epithelium which Contributes to Increased NEC Severity*

To determine whether perinatal CMV infection could increase NEC severity through TLR4 induction, we turned to the newborn mouse model and observed that mCMV infection significantly increased *Tlr4* expression in the ileum as compared with uninfected mice (Figure 6A). Furthermore, mCMV-infected newborn mice responded to LPS injection with significantly greater expression of *Tnf* in the ileum on postinfection day 7 as compared with uninfected mice (Figure 6B), consistent with an effect of CMV infection in enhancing TLR4 signaling in the intestine. In control experiments, we confirmed the specificity of an mCMV-mediated increase in TLR4 signaling in the small intestinal epithelium by repeating the mCMV infection studies in intestinal-specific *Tlr4*-knockout mice (*Tlr4*<sup>ΔIEC</sup>),<sup>24</sup> which did not increase *Tnf* expression in response to LPS and mCMV (Figure 6F). Conversely, TLR4-overexpressing mice that selectively overexpress *Tlr4* on the intestinal epithelium in a *Tlr4*-knockout background (*Tlr4*<sup>OVER</sup>) showed enhanced LPS-induced *Tnf* expression in the ileum, thus mimicking the effect of mCMV infection on increasing *Tlr4* expression and signaling (Figure 6F).

We next assessed whether the effect of CMV infection on increasing NEC severity occurs through increased TLR4 signaling, and thus performed studies on mice with 3 distinct genetic backgrounds (wild-type, *Tlr4*<sup>ΔIEC</sup>, and *Tlr4*<sup>OVER</sup>), which were each infected with mCMV at birth and then induced to develop NEC. As shown in Figure 6, the expression of *Tlr4* in the intestinal epithelium is required for NEC induction in response to mCMV infection, because *Tlr4*<sup>ΔIEC</sup> mice did not develop NEC, as shown by normal-appearing hematoxylin-eosin (H&E)-stained histologic sections in comparison with wild-type mice (Figure 6C and D) and a failure to induce *Tnf* expression (Figure 6F). By contrast, *Tlr4*<sup>OVER</sup> mice developed severe NEC even in the absence of mCMV infection, as indicated by H&E staining (Figure 6E) and *Tnf* expression in the intestinal epithelium (Figure 6F), mimicking the effects of mCMV on TLR4 expression in NEC development. Further confirmation that mCMV infection led to NEC via TLR4 induction is shown in Figure 6G-I, in which mCMV infection led to significantly increased DHE staining (reflective of increased reactive oxygen species [ROS] release) in wild-type mice with NEC that was not seen in *Tlr4*<sup>ΔIEC</sup> mice exposed to NEC, leading to significantly increased NEC severity scores in wild-type as compared with *Tlr4*<sup>ΔIEC</sup> mice. As anticipated, *Tlr4*<sup>OVER</sup> mice developed severe NEC, mimicking the effects of CMV infection in the wild-type mice (Figure 6J). Taken together, these data indicate that CMV infection leads to severe NEC at least in part through increased TLR4 expression.

### *CMV Infection Reduces Methylation of the TLR4 Promoter in Mice and Humans*

We next sought to investigate whether CMV might alter the degree of methylation of the TLR4 promoter as a mechanism by which the virus could increase TLR4 expression. To do so, we performed TLR4 promoter

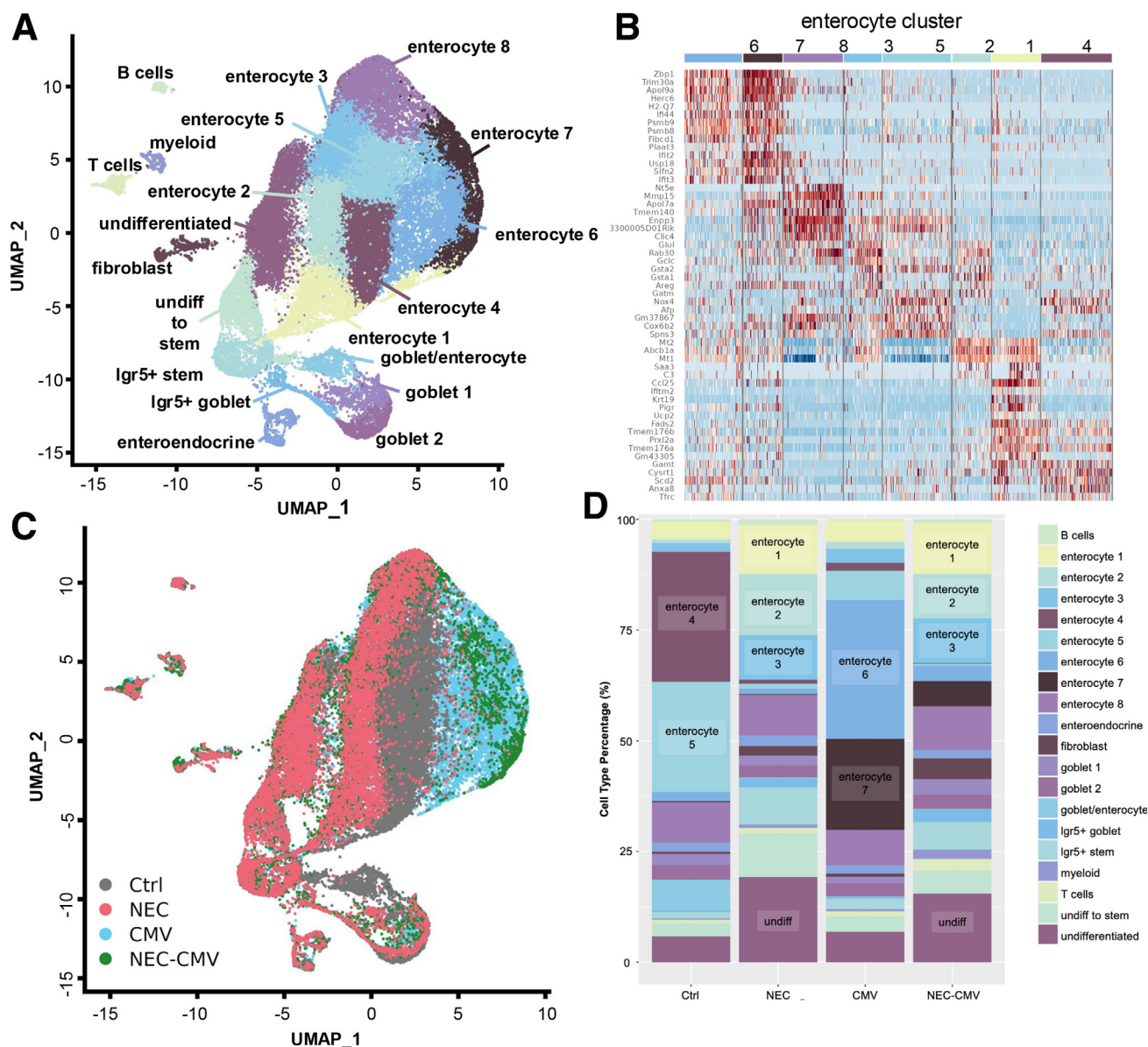


**Figure 3. Patterns of gene expression in the intestinal epithelium of CMV-infected mice.** Single-cell RNA sequencing was performed on the ileal mucosa of neonatal mice perinatally infected with murine CMV and induced to develop experimental NEC, n = 4 mice/group. (A) Uniform manifold approximation projection (UMAP) of integrated single-cell data from all 4 groups. (B) Heatmap of top differentially expressed genes for enterocytes. (C) UMAP projection colored by condition rather than cell type showing CMV and control enterocytes cluster distinctly from NEC-CMV and NEC enterocytes. (D) Bar graph showing the percentage of each cell type by condition, thus quantifying the difference between enterocyte subtype expression for each condition.

methylation studies via methylation-specific qPCRs on the genomic DNA isolated from tissue and cells infected with mCMV, using primer pairs designed to target the *TLR4* promoter region (Table 1). As shown in Figure 7, mCMV infection significantly decreased the methylation index in genomic DNA samples that were isolated from the ileum from mice (Figure 7Ai). To assess whether these effects could be observed independent of circulating immune cells, we next performed studies on enteroids derived from the ilea of mCMV-infected newborn mice (Figure 7Bi), which similarly revealed a decrease in methylation of the *TLR4*

promoter. To assess potential mechanisms governing the effects of CMV on *TLR4* methylation, we next assessed whether viral infection could alter the expression of DNA methyltransferase 1 (*Dnmt1*), an enzyme that catalyzes the transfer of methyl groups to specific CpG sites in the DNA.<sup>25</sup> CMV infection significantly reduced the expression of *Dnmt1* in mouse ileum and mouse ileal enteroids (Figure 7A and B) when compared with uninfected samples. These data suggest a potential mechanism by which CMV infection could increase *TLR4* expression through effects on methylation of its promoter.

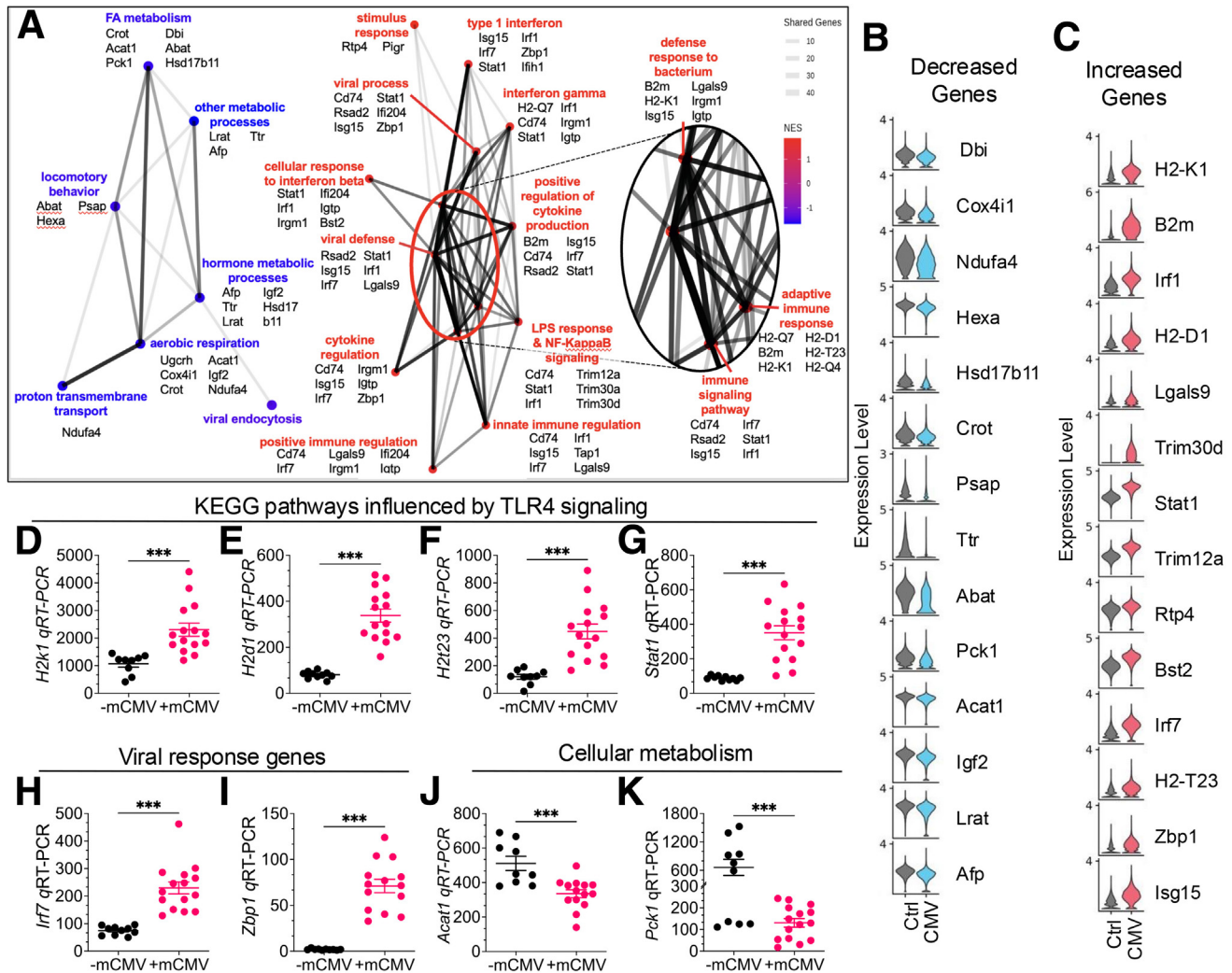


**Figure 4. Murine CMV infection increases the expression of genes related to immune response pathways and decreases the expression of genes related to energy metabolism profile in enterocytes.** (A) Network plot visualization of GSEA in CMV infected and uninfected (control) enterocytes reveals that CMV infection increases the expression of genes related to immune pathways and decreases the expression of genes related to cellular metabolic pathways. Similar gene ontology terms were manually combined and colored by average normalized enrichment score (NES) on a gradient scale from decreased enrichment (blue) to increased enrichment (red). Genes making the greatest contribution to pathway enrichment are listed below each combined term. The number of genes shared between terms is represented by the thickness and darkness of the line between pathways. (B, C) Stacked violin plots show the expression levels of significantly ( $P < .05$ , Wilcoxon rank sum test) differentially expressed genes contributing to the pathway enrichment in CMV mice versus control mice. The first stack represents genes that are downregulated (blue), and the second contains upregulated genes (red). (D-K) qPCR validation of single cells data. Kyoto Encyclopedia of Genes and Genomes (KEGG) pathways analysis showing genes influenced by TLR4 signaling. Histocompatibility 2, K region locus (2H2k1, D); histocompatibility 2, D region locus 1 (H2d1, E); histocompatibility 2, T region locus 23 (H2t23, F); and signal transducer and activator of transcription 1 (Stat1, G). Viral related genes: Interferon regulatory factor 7 (Irf7, H) and Z-DNA binding protein 1 (Zbp1, I). Energy metabolism: Acetyl-Coenzyme A acetyltransferase 1 (Acat1, J) and Phosphoenolpyruvate carboxykinase 1, cytosolic (Pck1, K). Statistical significance was determined by 1-way analysis of variance followed by Tukey's multiple comparisons tests or unpaired t-test using GraphPad Prism 10 software. \*\*\* $P < 0.001$ . Mice data from  $>8$  mice per group for PCR validation genes.

### Murine CMV Infection in Newborn Mice Induces TLR4-Dependent Mitochondrial Injury and Adenosine Triphosphate Depletion in NEC

CMV infection is known to target mitochondria where it can result in adenosine triphosphate (ATP) depletion in the host.<sup>26</sup> The subsequent impairment of mitochondria function would be expected to then release ROS, a

finding that is consistent with the increased DHE staining that we observed in the small intestine of CMV infected mice (Figure 20), and with the GSEA findings revealing a disruption in mitochondrial genes related to cellular metabolism (Figure 4). We therefore next investigated whether mCMV infection in newborn mice induces mitochondrial injury in the intestinal epithelium,



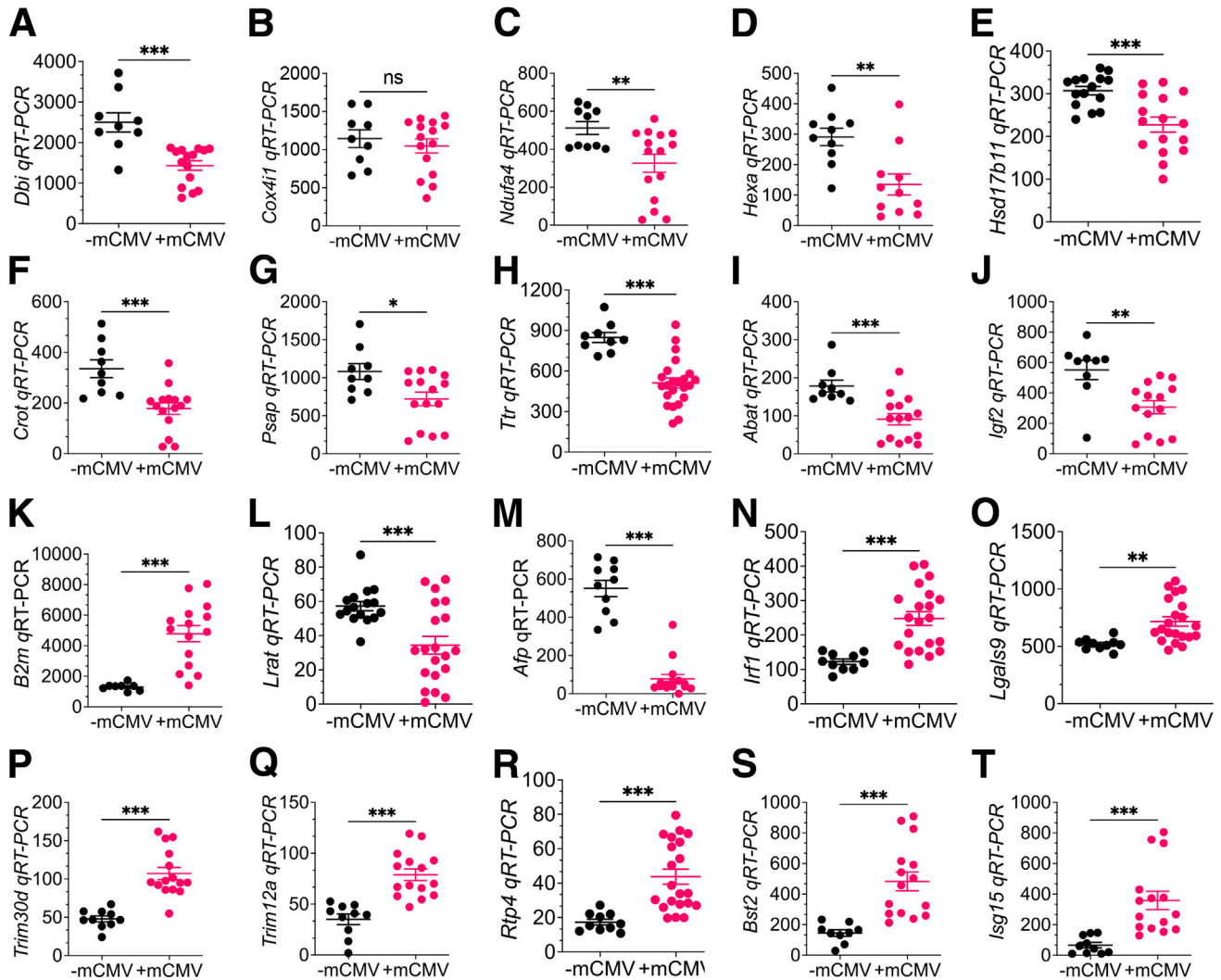


**Figure 5. Single-cell sequencing data validation by qRT-PCRs in the ileum of newborn mice.** (A–T) qRT-PCR expression of Diazepam-binding inhibitor, *Dbi* (A); Cytochrome c oxidase subunit 4I1, *Cox4i1* (B); *Ndufa4*, mitochondrial complex associated, *Ndufa4* (C); hexosaminidase A, *Hexa* (D); Hydroxysteroid (17- $\beta$ ) dehydrogenase 11, *Hsd17b11* (E); Carnitine O-octanoyltransferase, *Crot* (F); Prosaposin, *Psap* (G); Transthyretin, *Ttr* (H); 4-aminobutyrate aminotransferase, *Abat* (I); Insulin-like growth factor 2, *Igf2* (J); Beta-2 microglobulin, *B2m* (K); Lecithin-retinol acyltransferase (phosphatidylcholine-retinol-O-acyltransferase), *Lrat* (L); Alpha fetoprotein, *Afp* (M); Interferon regulatory factor 1, *Irf1* (N); Lectin, galactose binding, soluble 9, *Lgals9* (O); Tripartite motif-containing 30D, *Trim30d* (P); Tripartite motif-containing 12A, *Trim12a* (Q); Receptor transporter protein 4, *Rtp4* (R); Bone marrow stromal cell antigen 2, *Bst2* (S); ISG15 ubiquitin-like modifier, *Isg15* (T), on CMV<sup>-</sup> and CMV<sup>+</sup> mouse ileal tissues. Statistical significance was determined by unpaired t-test using GraphPad Prism 10 software. \* $P < .05$ , \*\* $P < .01$ , \*\*\* $P < .001$ , each dot is data from a different mouse,  $n = 9$  or more mice.

whether such mitochondrial injury could lead to NEC, and whether these changes occurred in a TLR4-dependent manner. Transmission electron microscopy of the ilea of wild-type mice without NEC that had been infected with mCMV revealed significant mitochondrial disruption, characterized by a loss of cristae and the formation of spherical inclusion bodies (Figure 8A and B), which are characteristic features of the effects of CMV on mitochondrial injury.<sup>27–29</sup> Importantly, mCMV infection in mice lacking *Tlr4* did not show any mitochondrial disruption (Figure 8C and D), suggesting that TLR4 plays a pivotal role in mediating mitochondrial injury in response to CMV infection in the intestinal

epithelium. CMV infection led to a significant induction in the mitochondrial fission gene *Drp1* ( $P < .001$ ) and the mitophagy gene *Pink1* ( $P < .01$ ) (Figure 8E and F), consistent with the transmission electron microscopy findings, while also leading to a TLR4-dependent induction in mtDNA fragmentation (Figure 8G). The effects of mCMV on the mitochondria also impacted cellular metabolism, because mCMV infection resulted in a significant reduction in ATP levels in the intestinal mucosa of wild-type ileum that was not observed in TLR4-deficient mice, confirming the role of TLR4 in mediating CMV-induced mitochondrial damage in the newborn intestine (Figure 8H).

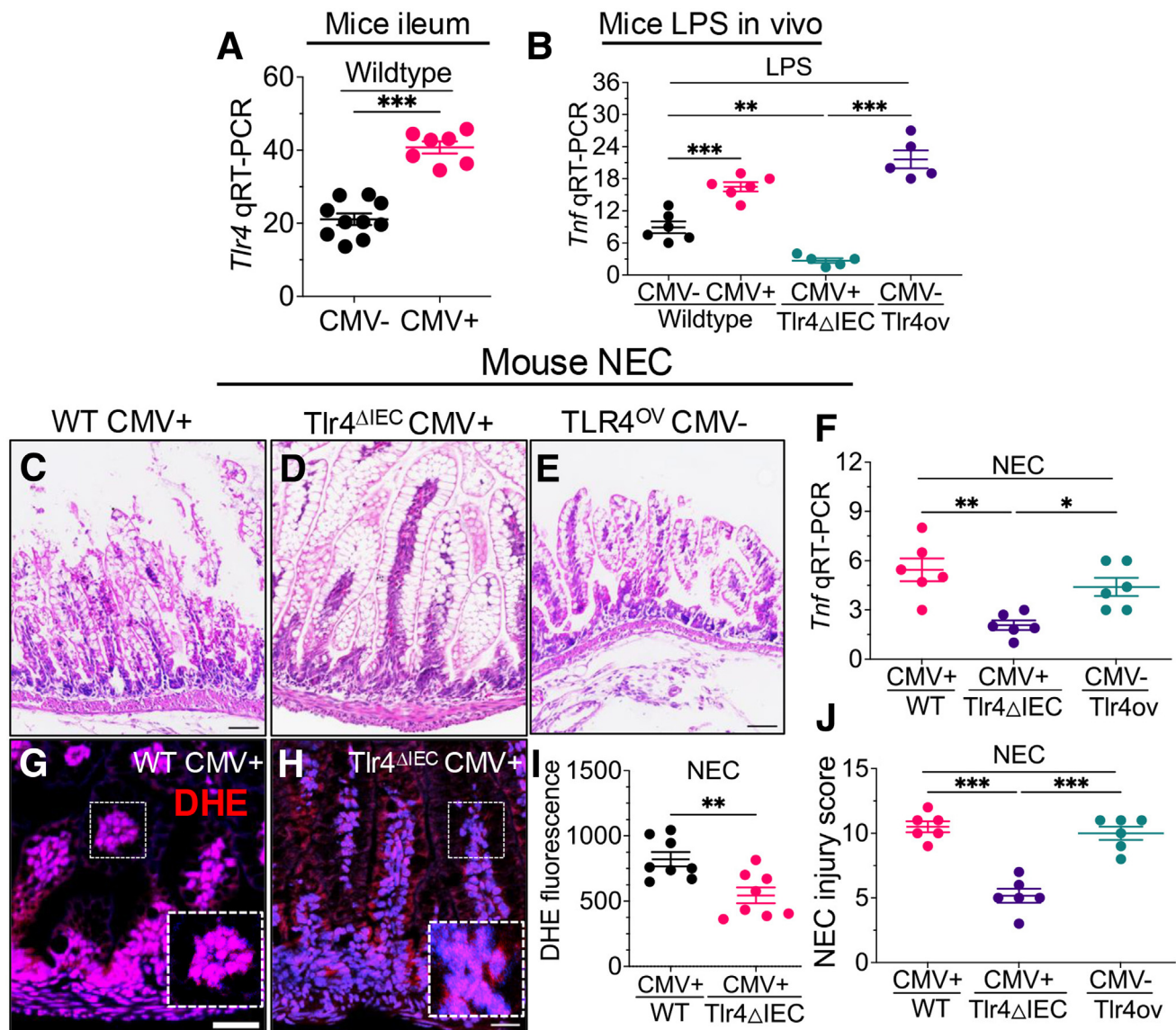


**Figure 6. Murine CMV infection in newborn mice leads to increased TLR4 signaling in the intestinal epithelium, which contributes to increased NEC severity.** (A) qRT-PCR of *Tlr4* in the ilea of mice with and without perinatal CMV infection. (B) *Tnf* expression in the ilea of neonatal mice perinatally infected with murine CMV and treated on postnatal day 7 with LPS (5 mg/kg, intraperitoneally, 6 hours). (C-E) Representative H&E images of samples of the intestinal epithelium from mice induced to develop NEC that were either wild-type (WT), intestinal-specific TLR4-knockout mice (Tlr4<sup>ΔIEC</sup>), or which overexpress TLR4 in the intestinal epithelium on a *Tlr4*<sup>-/-</sup> background (*Tlr4*<sup>OVER</sup>) and which were either infected (CMV+) or uninfected (CMV-) with CMV. (F) qRT-PCR expression of *Tnf* corresponding to the groups in C-E. (G, H) Representative confocal images and quantification using image J software (I) of the ROS marker DHE (red); DAPI is shown in blue. (J) NEC injury score as defined in Methods. Statistical significance was determined by 1-way analysis of variance followed by Tukey's multiple comparisons tests or unpaired t-test using GraphPad Prism 10 software. \**P* < .05, \*\**P* < .01, \*\*\**P* < .001. Scale bars = 50 μm. Mice data from 6–10 mice per group.

### CMV Infection Induces ATP Loss and Alters the mRNA Expression of Key Adenosine-ATP Homeostatic Enzymes

Shown in Figure 9A is an overview of the key molecules involved in the metabolism of ATP and its precursor adenosine within the cell. We observed that mCMV infection led to a significant reduction in ATP concentration in the ileal mucosa (black vs cyan dots in Figure 9B) that was further reduced in the presence of NEC (cyan vs purple dots in Figure 9B), consistent with the mitochondrial damage

induced by CMV. The effects of CMV in reducing ATP production were also observed in cultured intestinal epithelial cells (IEC-6), which were infected with mCMV for 48 hours, and which resulted in a significant decrease in ATP synthesis compared with uninfected cells (Figure 9C). In seeking to understand how CMV could reduce ATP synthesis, we next assessed key ATP synthetic enzymes, transporters, and receptors in the intestines of mice with and without mCMV infection in the presence or absence of NEC. mCMV infection significantly reduced the expression of the

**Table 1.** Primer Sequences Used in the Current Study (Forward and Reverse)

<b>qRT-PCR primers</b>	
<i>Abat (mouse)</i>	GAGCTGGAGACTTGCATGGT; GCTAAGCAACCCATGGTCCT
<i>Acat1 (mouse)</i>	AGCTGTTTCTCTGGGCCATC; CCTCCTCCTCCGTTGCAAAT
<i>Ada (mouse)</i>	AGATGAAGGCAAAGGAGGGC; CGTCCCCTTCAGTCTGGTTC
<i>Adk (mouse)</i>	CAAGGGCGAGATGACACCAT; GCATCTCCAGTCCATGGT
<i>Adora1 (mouse)</i>	ATCCTCACCCAGAGCTCCAT; CGCTGAGTACCACTGTCTT
<i>Adora2a (mouse)</i>	TGCTTTGTCTGGTCCCTCAC; AAGCCATTGTACCGGAGTGG
<i>Adora2b (mouse)</i>	TCTTTAGCCTCTTGGCGGTG; CAGCAATGATCCCTCTCGT
<i>Adora3 (mouse)</i>	GTCTGTGTGTGCTGCTGATCT; TGAGTGGTAACCGTTCTATATCTGA
<i>Afp (mouse)</i>	AAACCTCCAGGCAACAACCA; TTCCTTGGCAACACTCCTCG
<i>Ahcy (mouse)</i>	ACAAACCAGGTGATGGCACA; GCTTCACATTACAGCTTGCCC
<i>B2m (mouse)</i>	ATGGCTCGCTCGGTGACCCT; TTCTCCGGTGGGTGGCGTGA
<i>Bst2 (mouse)</i>	GTCACGAAGCTGAACCAGGA; AGTAGGCTGGAGACCAACAT
<i>Cd39 (mouse)</i>	GACTACGAACAGTGCCACCA; GAAAACGCCCAAACTCCC
<i>Cd73 (mouse)</i>	TCCTGCAAGTGGGTGGAATC; AGATGGGCACTCGACACTTG
<i>Cnt1 (mouse)</i>	GTCCAAGTCCGGAGTGAGG; GCAATGTTGGCAACGACCTT
<i>Cnt2 (mouse)</i>	ATGTGTGCTGCAGAGAGCTT; GCAAGATTCTGAGGCTGGA
<i>Cnt3 (mouse)</i>	GTCACGATGGGGTCATCTCC; CGACTTGGTGACGTGTGGTA
<i>Cox4i1 (mouse)</i>	TCACTGCGCTCGTTCTGATT; TGGCCTTCATGTCCAGCATT
<i>Crot (mouse)</i>	TTCAGGGTGTGTGGTTCCC; TCCAGGATGAACATGCCACC
<i>Dbi (mouse)</i>	AAACAAGCTACTGTGGGCGA; TCAGCTTGTTCACAGTCC
<i>Dnmt1 (mouse)</i>	GAGGCCACTGTCTGGTTC; AGCTTATGGGCTATGACGCC
<i>Drp1 (mouse)</i>	TGCCAGCAAGTCCACAGAAA; ACAATCTGCTGTTCTCGGG
<i>Ent1 (mouse)</i>	GCAGAGCAGGAGACCAAGTT; GGTTCCTGTTGGTGGGTGGA
<i>Ent2 (mouse)</i>	TGCCCATCATCTTCAGGCAG; CCTCTCATGTGGCAACACCT
<i>Ent3 (mouse)</i>	CCTTCTCTCATGGCAGCA; GGCAACTGGCCTCATGTAGT
<i>Ent4 (mouse)</i>	ATGTGCGATCCGGAGACATC; CGCATGTAGACCCCACTGTT
<i>H2d1 (mouse)</i>	ATGCCGTGTGTACCATGAGG; ACACCCAGAACAGCAACGAT
<i>H2K1 (mouse)</i>	ATCTGTGGTGGTGCCTCTTG; GCCATGTTGGAGACAGTGGA
<i>Ht2t23 (mouse)</i>	CGCTGGGAAATGAGACACT; CAGCACCTCAGGGTCACTTC
<i>Hexa (mouse)</i>	ATTGGAGGGGAGGCCTGTAT; CTGCTCCACAGTCTCTCAGC
<i>Hsd17b11 (mouse)</i>	CAGCGCTGCGAAAAAGGTAA; GAGGGTCTGCGTAGCAAAT
<i>Ilf6 (mouse)</i>	CCAATTTCCAATGCTCTCCT; ACCACAGTGAGGAATGTCCA
<i>Irfng (mouse)</i>	AGGCCATCAGCAACAACATAAGCG; TGGGTTGTTGACCTCAAACCTGGC
<i>Igf2 (mouse)</i>	TTCCGAGATGTCCAGCAACC; TGTGGGACGTGATGGAAGT
<i>Irf1 (mouse)</i>	GAAAGTCCAAGTCCAGCCGA; GCTGTGGTCATCAGGTAGGG
<i>Irf7 (mouse)</i>	AGGTTCTGCAGTACAGCCAC; GGGTTCCTCGTAAACACGGT
<i>Isg15 (mouse)</i>	AAGCAGCCAGAACGAGACTC; TCACGGACACCAAGAAATCG
<i>Lgals9 (mouse)</i>	ATGGGCTTTACCCGTTCCAAAG; ATGTCACTCCACAGGCAAG
<i>Lrat (mouse)</i>	GCTCTCGGATCAGTCCACAG; TGCTAATCCCAAGACAGCCG
<i>Ndufa4 (mouse)</i>	AAACATGCTCCGCCAGATCC; GCCAAGCGCATCACATACAG
<i>Pck1 (mouse)</i>	TGGAAGGTGCAATGTGTGGG; CTTCACTGAGGTGCCAGGAG
<i>Pink1 (mouse)</i>	GTGGACCATCTGGTTCAGCA; GATCACTAGCCAGGGACAGC
<i>Psap (mouse)</i>	TCCAGGCCCAATGTGATT; GGAGCTCCTCAGTGGCATT
<i>Rtp4 (mouse)</i>	GCTATGAGATACAAAGCGGCG; CCAGGTCTGTACGTGGCAT
<i>Stat1 (mouse)</i>	CTGCTGTGCCTCTGGAATGA; TGAATGTGATGGCCCCCTTC
<i>Tlr4 (mouse)</i>	TTTATTGAGAGCCGTTGGTG; CAGAGGATTGCTCTCCATT
<i>Tlr4 (rat)</i>	ACTGGGTGAGAAACGAGCTGGTA; AAGCCTTCTGGATGATGTTGGCA
<i>Tnf (mouse)</i>	TTCCGAATTCACTGGAGCCTCGAA; TGCACCTCAGGGAAGAATCTGGAA
<i>Trim12a (mouse)</i>	GAAGAAGCCCAAGCCATCG; ATGAGCCTCTGTGACCTTGC
<i>Trim30d (mouse)</i>	CAGAGGGAGTTGGTGAGAGAC; TTCAGTGTATGGTCTGAATGC
<i>Ttr (mouse)</i>	GCCTCGCTGGACTGGTATTT; CGGACAGCATCCAGGACTTT
<i>Rplp0</i>	GGCGACCTGGAAGTCCAACCT; CCATCAGCACCACAGCCTTC
<i>Zbp1 (mouse)</i>	GGCAGAAGCTCCTGTTGACT; TTCACCAGCTGGCCAATCTT
<b>Cytomegalovirus primers</b>	
<i>le1 (mouse CMV)</i>	AGCCACCAACATTGACCACGCAC; GCCCAACCAGGACACACAACCTC
<b>Mitochondrial damage primers</b>	
<i>mtDNA (short, human)</i>	CCCTAATAATCGGTGCCCCC; CAGATGCGAGCAGGAGTAGG
<i>mtDNA (long, human)</i>	AGGGTTGGTCAATTTCTGTGC; GAGCCTAGGGTGTGTGAGT
<i>mtDNA (short, mouse)</i>	ACGAGGGTCCAACTGTCTCTTA; TAGGGTAACCTGGTCCGTTGAT
<i>mtDNA (short, mouse)</i>	ACGAGGGTCCAACTGTCTCTTA; GCCCAGGAAATGTTGAGGGA
<b>Methylation-specific PCRs primers</b>	
<i>T14 promoter methylated (mouse)</i>	AGAAAGTATTATGATATAAGATACGG; TTAATAAAAAACAAAAAATAACGTA
<i>Tlr4 promoter Unmethylated (mouse)</i>	AAAGAAAGTATTATGATATAAGATATGG; TTAATAAAAAACAAAAAATAACATA

qRT-PCR, quantitative reverse transcription polymerase chain reaction.



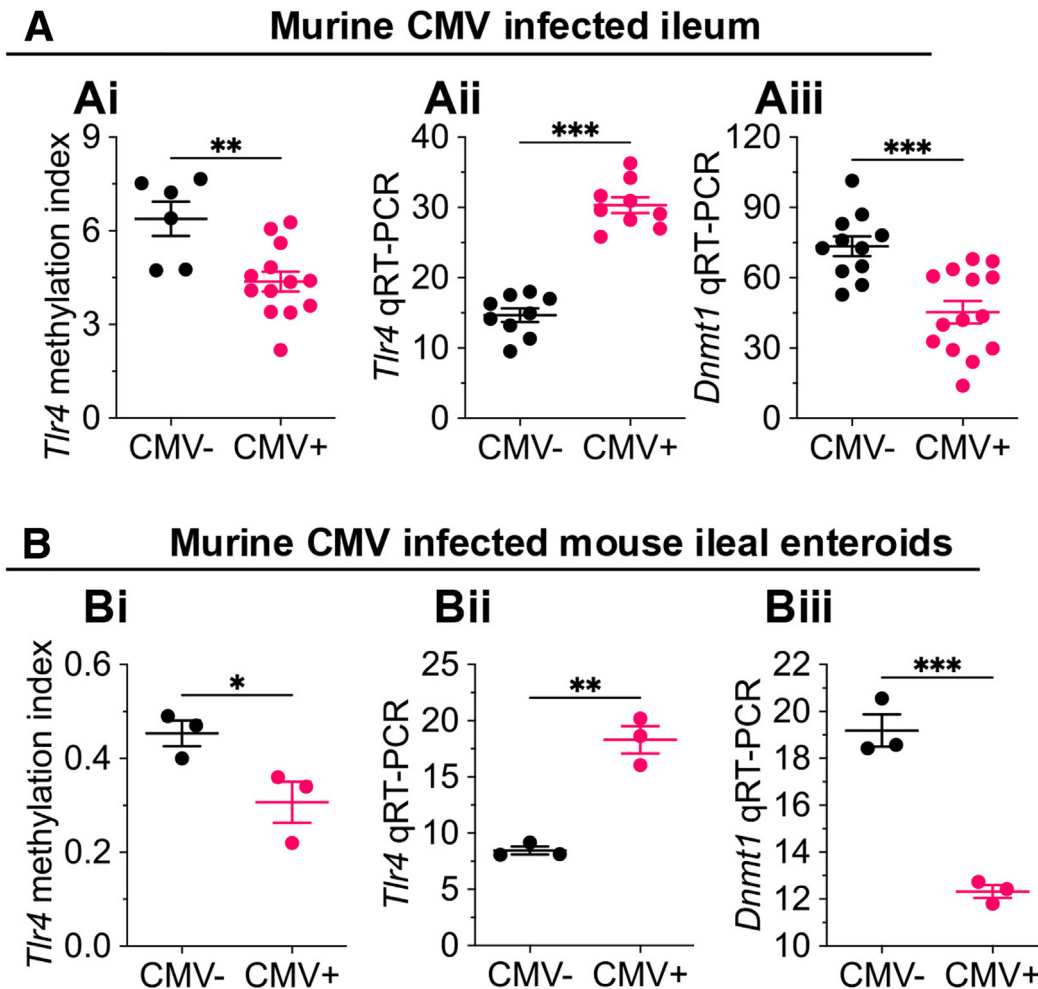


**Figure 7. CMV infection reduces methylation of the *TLR4* promoter in mice.** (A, B) *TLR4* promoter methylation index as calculated by methylation-specific PCRs on genomic DNA extracted from murine CMV infected mice ilea and murine CMV-infected mouse ileal enteroids and corresponding expression of *Tlr4* and *Dnmt1* (DNA methyltransferase 1) expression by qRT-PCRs on the corresponding indicated group. Statistical significance was determined by unpaired t-test using GraphPad Prism 10 software. \* $P < .05$ , \*\* $P < .01$ , \*\*\* $P < .001$ , each dot is data from a different mouse or human specimen or enteroids culture well.  $n \geq 9$  human specimens or mice/group,  $n = 3-4$  enteroids wells.

ATP synthesis enzyme, ATP synthase F1 subunit alpha (*Atp5a1*) in newborn mice, and these levels remained low in the presence of NEC (Figure 9D), although there was no effect of the expression of *Adk1* (Figure 9E). Conversely, mCMV infection increased the mRNA expression of the ATP catabolism enzymes *Entpd1/Cd39* and *Nt5e/Cd73*, which are involved in the extracellular generation of adenosine (Figure 9F and G), whereas the expression of both enzymes were reduced in ileal NEC tissues independent of mCMV infection status (Figure 9F and G). The expression of S-adenosylhomocysteine hydrolase (*Ahcy*) which governs the alternate intracellular route of adenosine generation via S-adenosylhomocysteine, did not change after mCMV infection (Figure 9H), whereas the expression of adenosine deaminase (*Ada*), which promotes the catabolism of adenosine to inosine, was significantly increased after mCMV infection (Figure 9I). The expression levels of key transporters and adenosine receptors in response to CMV infection and NEC induction are shown in Figures 10 and 11, and suggest that

CMV infection dysregulates the ATP/adenosine metabolism by reducing ATP synthesis and increasing adenosine catabolism. We therefore next assessed whether supplementation with a highly selective adenosine receptor agonist NECA could protect against NEC development.

#### Supplementation with the Adenosine Receptor Agonist NECA Reverses the Effects of CMV Infection on the Development of NEC in Mice

In the next series of experiments, we sought to reverse the effects of CMV infection on mitochondrial injury as a strategy to attenuate NEC. To do so, we supplemented the infant formula in the NEC model with the adenosine receptor agonist NECA, in both mCMV infected and uninfected mice. As shown in Figure 12A-D, NECA supplementation reversed the marked histologic impairment in the intestinal mucosa (Figure 12B and D), attenuated the induction of *Tnf* (Figure 12E), and reduced the induction in the expression of 3'-NT observed in the intestinal

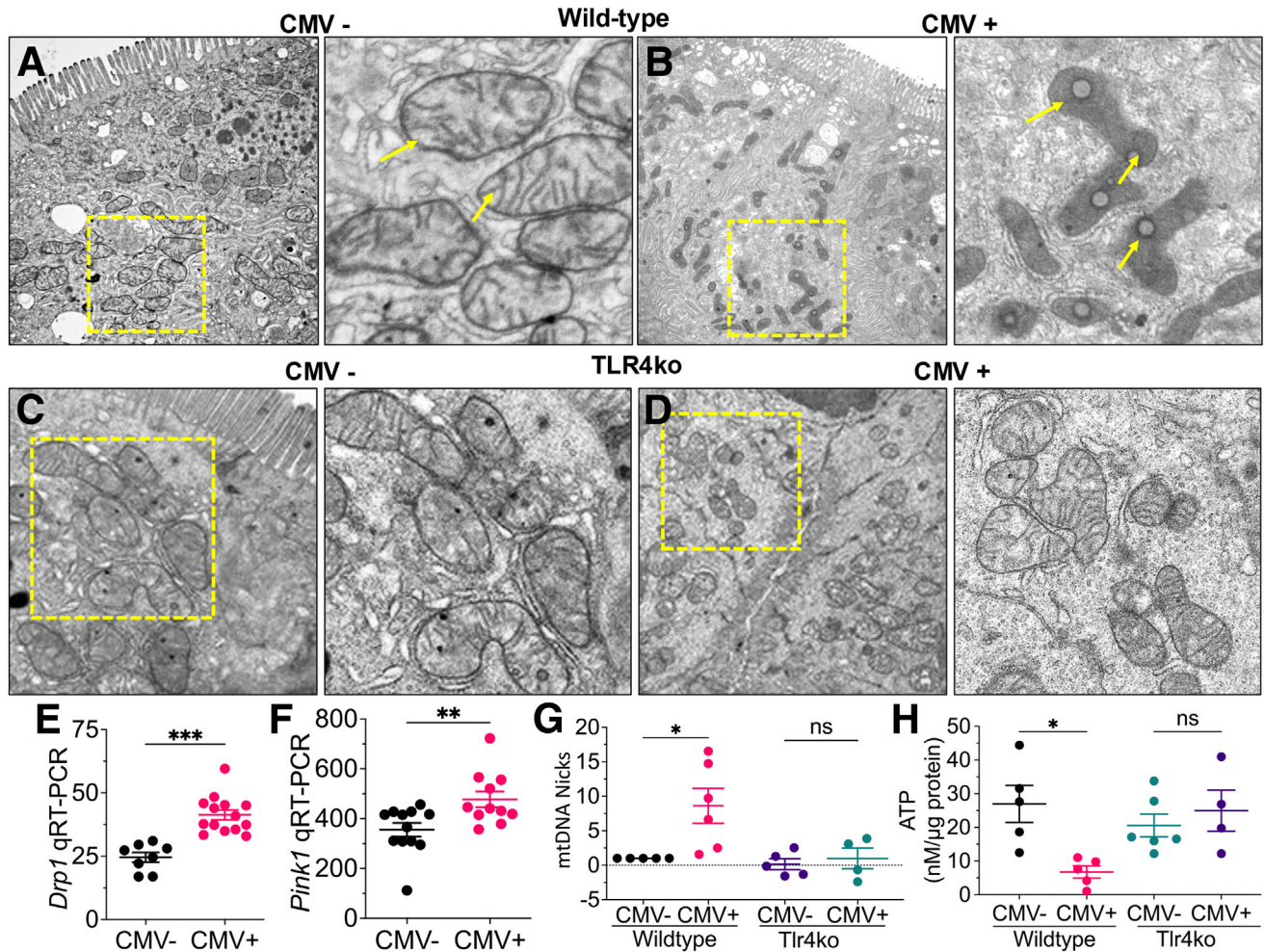


**Figure 8. Murine CMV infection in newborn mice induces TLR4-dependent mitochondrial injury and ATP depletion in NEC.** (A-D) Representative transmission electron microscope images of the terminal ileum in wild-type (A, B) or TLR4 knockout (TLR4<sup>ko</sup>, C, D) mice that were either uninfected (A, C) or perinatally infected with mCMV (B, D). A magnified area corresponds to the yellow region in each image. (E, F) *Drp1* and *Pink1* expression by qRT-PCR in the terminal ilea of wild-type mice with and without mCMV infection. (G) mtDNA nicks using qPCR on genomic DNA in the indicated group. (H) ATP concentrations in the terminal ileum in the indicated group; \**P* < .05, \*\**P* < .01, \*\*\**P* < .001, each dot represents a separate mouse; 3 separate experiments. Transmission electron microscope at x800.

mucosa of mice with NEC (Figure 12F-J). Finally, because we have shown that CMV increases *Tlr4* expression and signaling (Figures 6 and 7), we also sought to determine whether NECA administration could reverse the effects of mCMV on TLR4 signaling and expression in the intestinal epithelium. As shown in Figure 13, treatment of IEC-6 enterocytes with mCMV for 48 hours resulted in increased LPS-induced translocation of nuclear factor kappa B (NF- $\kappa$ B) from the cytoplasm to the nucleus (Figure 13A, B, E, and M), which was increased further in the presence of mCMV pretreatment (Figure 13E and M) and reduced in the presence of NECA (Figure 13D and F). Similarly, TLR4 activation by LPS led to an increase in DHE staining (reflective of ROS generation) in IEC-6 enterocytes (Figure 13G, H, and N), which was increased by mCMV (Figure 13K and N) and reduced in the presence of NECA (Figure 13L and M). The NECA-mediated protection against CMV-induced TLR4 signaling correlated with a parallel reduction in expression of *Tlr4* (Figure 13O) and the downstream cytokine *Tnf*

(Figure 13P). Of note, the infectivity of mCMV in IEC-6 cells was confirmed by induction of *Ie1* (Figure 14). The observations that NECA treatment can attenuate the effects of CMV infection on TLR4 signaling in cultured enterocytes were also observed in the intestinal epithelium of newborn mice. Specifically, LPS treatment of mice resulted in increased DHE staining (Figure 13Q, R, and W), and the expression of NADPH oxidase activator 1 (*Noxa1*, Figure 13X), and *Tlr4* (Figure 13Y) and the downstream molecule *Tnf* (Figure 13Z), which were all reduced in the presence of NECA treatment (Figure 13Q-Z). Taken together, these findings suggest that activation of the adenosine receptors can attenuate NEC by reducing the deleterious effects of CMV on mitochondrial function and by reversing the effects of TLR4 signaling within the intestinal mucosa.

## Discussion

This study provides 6 lines of evidence that CMV infection worsens NEC, which occurs through multiple

## A Adenosine/ATP metabolic and signaling pathway

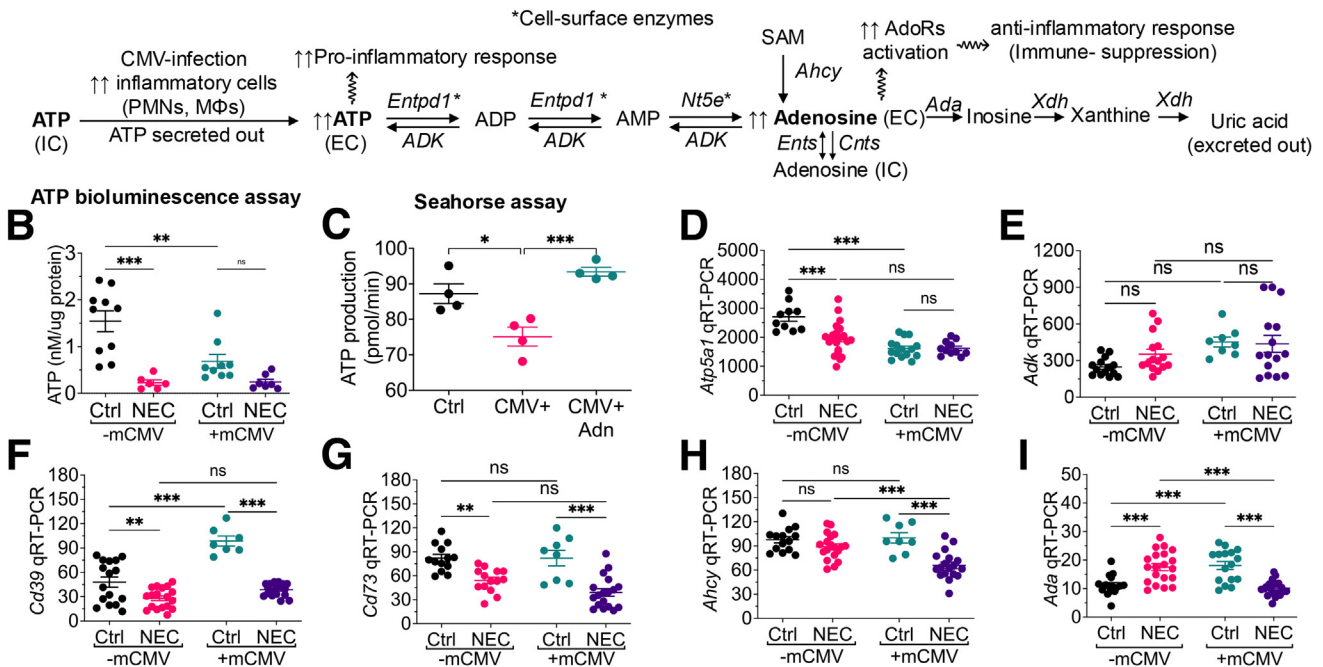


**Figure 9. CMV infection induces ATP loss and alters the mRNA expression of key adenosine-ATP homeostatic enzymes.** (A) A schematic illustration of the adenosine/ATP metabolic homeostasis pathway. (B) ATP levels in the small intestinal mucosa of newborn mice with and without NEC in the presence or absence of mCMV infection as indicated. (C) ATP generation as measured via the Seahorse assay in IEC6 cells infected with CMV and treated with the adenosine receptor agonist NECA. (D–I) qRT-PCR expression of the following genes in the intestinal mucosa of ctrl or NEC mice in the presence or absence of mCMV infection: ATP synthesis genes, ATP synthase F1 subunit alpha (*Atp5a1*, D), adenosine kinase (*Adk*, E); the Ectonucleotidases, ectonucleoside triphosphate diphosphohydrolase 1, (*Entpd1*, F) and 5' nucleotidase, ecto, (*Nt5e*, G); Adenosylhomocysteinase (*Ahcy*, H); adenosine deaminase (*Ada*, I). ATP, Adenosine triphosphate; ADP, Adenosine diphosphate; AMP, Adenosine monophosphate; Adn, Adenosine; IC, intracellular; EC, Extracellular; ADK, Adenosine kinase; ADA, Adenosine deaminase; AdoRs, Adenosine receptors; *Ador2a*, Adenosine receptor 2a; *Xo*, Xanthine Oxidase. Each dot in the graph is a different mouse data. Statistical significance was determined by 1-way analysis of variance followed by Tukey's multiple comparisons tests using GraphPad Prism 10 software. ns, nonsignificant, \* $P < .05$ , \*\* $P < .01$ , \*\*\* $P < .001$ .

mechanisms: (1) increased NEC severity in CMV-infected mice; (2) altered gene expression in CMV-infected murine enterocytes, with increased immune response and decreased metabolic activity; (3) CMV infection increases

*Tlr4* expression and hypomethylation of the *Tlr4* promoter; (4) CMV-induced mitochondrial injury exacerbated NEC severity; (5) mice in which *Tlr4* had been deleted from the intestinal epithelium did not exhibit mitochondrial injury

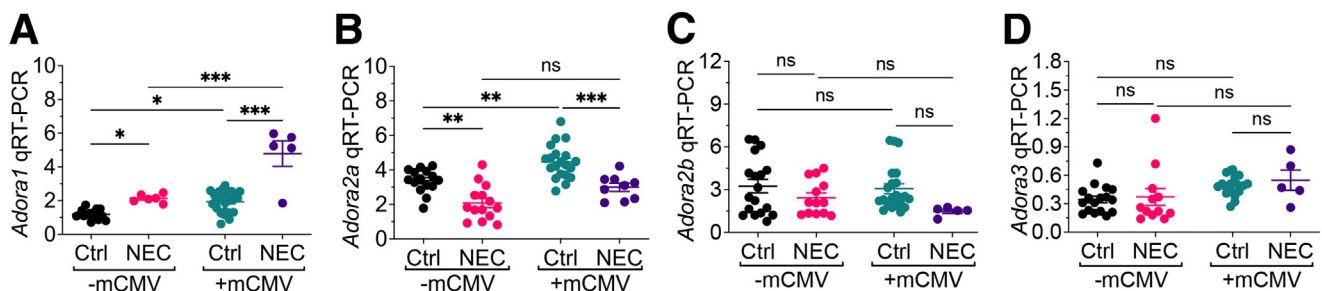


**Figure 10. Adenosine receptor expression in murine CMV-infected newborn mice induced to develop NEC with and without the adenosine receptor agonist, NECA.** (A–D) qRT-PCR expression of adenosine A1 receptor, *Adora1* (A); adenosine A2 receptor a, *Adora2a* (B); adenosine A2 receptor b, *Adora2b* (C); adenosine A3 receptor, *Adora3* (D) in the ileal tissues of uninfected (CMV-) and murine CMV-infected (CMV+) mice induced to develop NEC. Each dot in the graph is a different mouse data. Statistical significance was determined by 1-way analysis of variance followed by Tukey's multiple comparisons tests or unpaired t-test using GraphPad Prism 10 software. ns, nonsignificant ( $P > .05$ ), \* $P < .05$ , \*\* $P < .01$ , \*\*\* $P < .001$ . Each dot is a different mouse,  $n = 5$  or more mice.



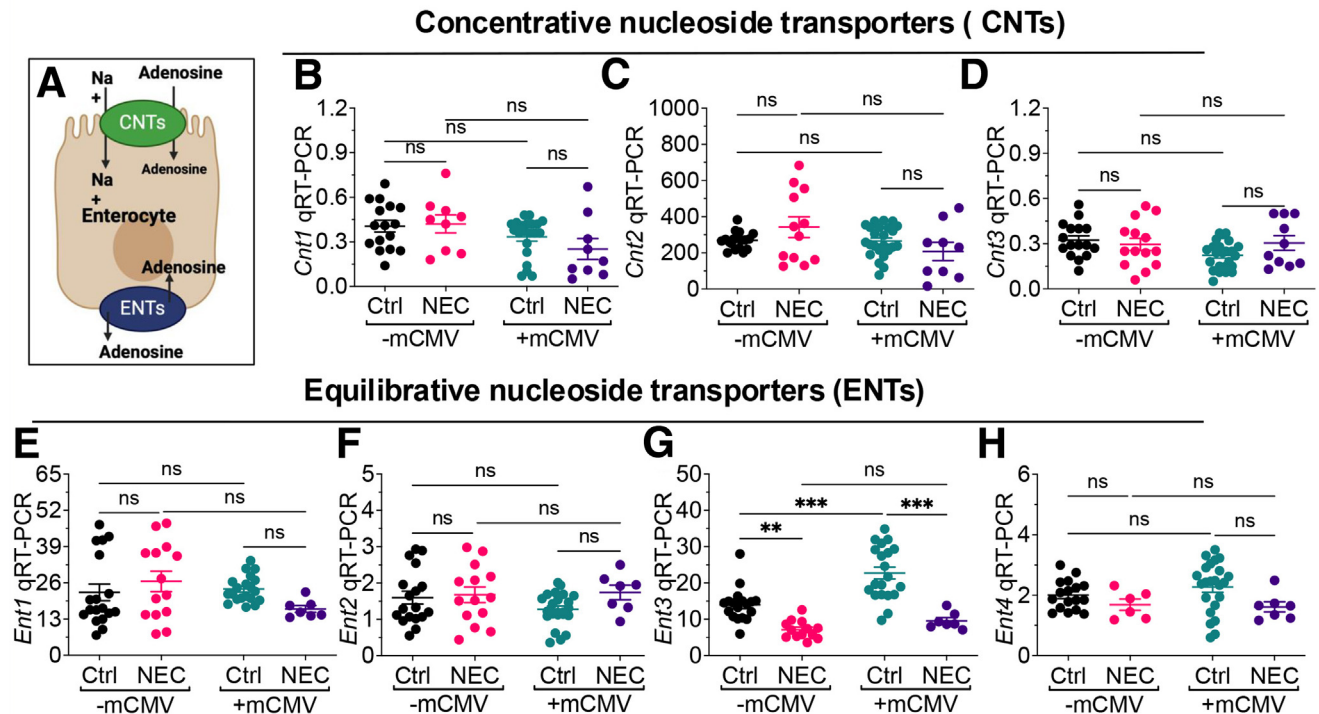


**Figure 11. Adenosine transporter expression in murine CMV infected mice induced to develop NEC with and without the adenosine receptor agonist, NECA.** (A) An illustration of concentrative nucleoside transporter (CNTs) and equilibrative nucleoside transporter (ENTs) on the intestinal epithelial cells. (B-D) qRT-PCR of the expression of *Cnt1*, *Cnt2*, and *Cnt3* and (E-H) *Ent1*, *Ent2*, *Ent3*, and *Ent4* in the ileal tissues of uninfected (CMV-) and murine CMV-infected (CMV+) mice induced to develop NEC. Each dot in the graph is a different mouse data. Statistical significance was determined by 1-way analysis of variance followed by Tukey's multiple comparisons tests or unpaired t-test using GraphPad Prism 10 software. \* $P < .05$ , \*\* $P < .01$ , \*\*\* $P < .001$ . Each dot is a different mouse,  $n = 5$  or more mice.

when infected with CMV; and (6) supplementation with the adenosine receptor agonist NECA reduced NEC severity after CMV infection by reducing NF- $\kappa$ B nuclear translocation,

and decreasing CMV-induced mitochondrial injury. Collectively, these findings suggest that CMV infection contributes to NEC severity by enhancing TLR4 signaling and causing

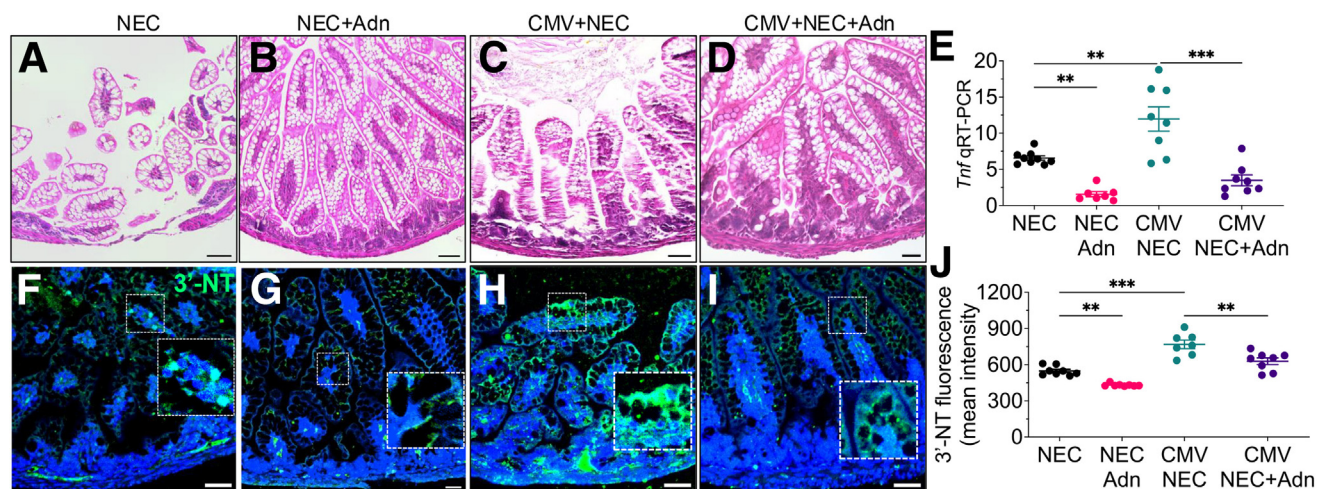


**Figure 12. Adenosine supplementation reverses the effects of CMV infection on the development of NEC in mice.** CMV-infected newborn mice were induced to develop NEC with or without supplementation of the adenosine receptor agonist, NECA in the formula. (A-D) representative H&E images of terminal ileal sections. (E) qRT-PCR of *Tnf*. (F-I) Representative confocal images showing staining for the oxidative-injury marker 3'-nitrotyrosine (3'-NT, green; DAPI blue). (J) Quantification of 3'-NT staining using ImageJ software. Each dot in the graph is a different mouse data. Statistical significance was determined by 1-way analysis of variance followed by Tukey's multiple comparisons tests using GraphPad Prism 10 software. \*\* $P < .01$ , \*\*\* $P < .001$ . Scale bar 50  $\mu$ m.

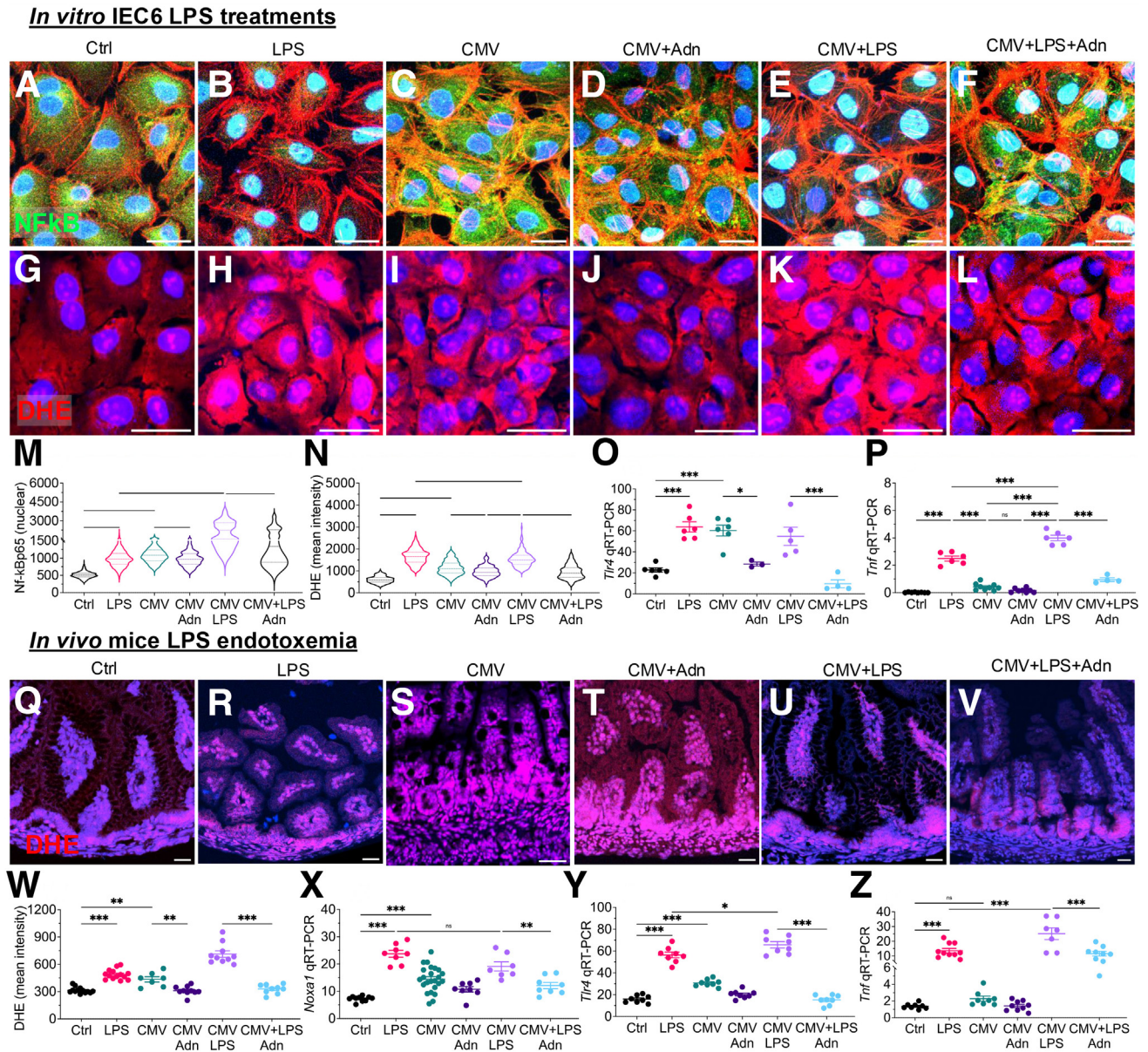


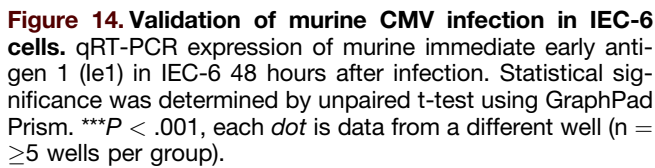
**Figure 13. Exogenous administration of the adenosine receptor agonist NECA reverses CMV-induced aberrant TLR4 signaling in murine CMV-infected cultured enterocytes and newborn mice.** *In vitro* IEC-6 cells: (A-L) Representative confocal images in cultured IEC-6 enterocytes treated with CMV for 24 hours, and 30-minute pretreatment with NECA (1  $\mu$ g/mL) before stimulation with LPS (50  $\mu$ g/mL, 6 hours) showing NF- $\kappa$ B translocation using anti-p65NF- $\kappa$ B antibody immunostaining (NF- $\kappa$ B, green; DAPI, blue; actin, red; A-F) and the reactive oxygen marker (ROS) marker DHE (DHE, red; DAPI, blue; G-L). (M, N) Violin plots showing the quantification of NF- $\kappa$ B (M) and DHE (N). (O, P) qRT-PCR for *Tlr4* and *Tnf*. *In vivo* C57-BL/6 mice: Newborn mice were infected with murine CMV and treated with LPS (5 mg/kg, intraperitoneally, 6 hours) on Day 7 with or without cotreatment with the adenosine receptor agonist, NECA (10 mg/kg, intraperitoneally). (Q-V) Representative confocal images showing staining for the reactive oxygen marker (ROS) marker dye DHE (DHE, red; DAPI, blue) under the indicated condition. (W) DHE quantification. (X-Z) qRT-PCR of NADPH oxidase activator 1, *Noxa1* (X), *Tlr4* (Y), and *Tnf*; (Z). Statistical significance was determined by 1-way analysis of variance followed by Tukey's multiple comparisons tests or unpaired t-test using GraphPad Prism 10 software. \* $P < .05$ , \*\* $P < .01$ , \*\*\* $P < .001$ . Each dot is a mouse or well; 3 separate experiments. Scale bar 10  $\mu$ m (A-P), scale bar 50  $\mu$ m (Q-V).

mitochondrial dysfunction, which was reversed with exogenous adenosine receptor activation.

One of the central findings of this study is that CMV infection increases TLR4 expression and causes mitochondrial dysfunction in the intestinal epithelium. These

processes seem to be linked to each other, because they were absent in mice deficient in *Tlr4*. CMV's negative impact on mitochondria aligns with prior studies,<sup>30–32</sup> and may explain its role in various congenital anomalies after in utero infection. Importantly, the production of ROS because





A significant finding of this study is that administration of an adenosine receptor agonist can reverse CMV-induced NEC severity in mice, possibly by bypassing virus-induced mitochondrial defects or inhibiting TLR4 signaling. It is noteworthy that mitochondrial injury may be linked to TLR4 signaling, because the induction of ROS has been shown to be a powerful promoter of TLR4 induction.<sup>38</sup> Although NECA is not currently used in clinical practice, adenosine is used in cardiovascular disease management. However, the use of adenosine in premature infants with NEC warrants caution because of the potential risk of cardiac toxicity, although such effects were not observed in the current study. Further optimization may be needed to enhance NECA's intestinal-specific properties.

NEC, suggesting its broader application even without CMV infection.

In summary, this study identifies CMV infection as a factor that worsens NEC severity by enhancing TLR4 signaling and causing mitochondrial dysfunction in the intestinal epithelium of mice. Furthermore, treatment with the adenosine receptor agonist NECA can reverse the effects of CMV infection on NEC induction by modulating mitochondrial function and attenuating TLR4 signaling effects. These findings provide new insights into the pathogenesis of NEC and suggest novel approaches to treatment.

### Study Design

*Mice*

C57BL/6J mice (stock no: 000664) and B6.SJL-Tg(Vilcre)997Gum/J9 (Stock no. 004586) were obtained from the Jax labs and bred in-house for multiple generations to stabilize the microbiota. TLR4 mutant mice either lacking TLR4 on the IEC (*Tlr4*<sup>ΔIEC</sup>) or overexpressing TLR4 on the IEC on a *Tlr4*<sup>null</sup> background (*Tlr4*<sup>ΔOVER</sup>) were generated in



our laboratory as previously described.<sup>24,44</sup> All mice were housed in a specific pathogen-free environment on a 12-hour-light/12-hour-dark cycle with free access to water and standard rodent chow (Teklad global 18% protein rodent diets, Envigo). All mice were genotyped before and after models to verify their correct genotypes.

### Antibodies, Reagents, Primers, and Kits

Antibodies included anti-m123/IE1 mCMV antibody (catalog no. HR-MCMV-12, Center for Proteomics), anti-3'-NT (catalog no. Ab61392, Abcam), and DHE (catalog no. D7008, Sigma-Aldrich).

Reagents included LPS from *Escherichia coli* 0127: B8 (catalog no. L3129, Sigma-Aldrich), 6-diamidino-2-phenylindole, dihydrochloride (DAPI, catalog no. D9542, Sigma-Aldrich), and 5'-N-Ethylcarboxamido adenosine (catalog no. E2387, Sigma-Aldrich).

Forward and reverse primers (Table 1) were custom-designed using National Center for Biotechnology Information Primer-BLAST online program and ordered from Integrated DNA Technologies.

Assay kits included RNAeasy Kit (catalog no. 74106, Qiagen), QuantiTect Reverse Transcription (catalog no. 205313, Qiagen), QIAamp DNA Kits (catalog no. 56304), and ATP determination kit (catalog no. A22066, Molecular Probes).

### Infection of Mice with Murine CMV

The mCMV/Murid beta-herpesvirus 1 (ATCC VR-1399) was obtained from the American Type Culture Collection (ATCC) and amplified to high titer ( $\sim 5 \times 10^6$  PFU/mL) in mouse embryonic fibroblasts (ATCC SC-1 CRL-1404). For mCMV infection in utero and/or at birth, 4 different methods were used to maximize the effectiveness of infection and to minimize technical shortcomings. (1) Ultrasound-guided in utero intrachorionic villi placental injections: Time-pregnant dams (embryonic day, e17.5) underwent a laparotomy using aseptic conditions to eviscerate the cervix. Fifty microliters of mCMV ( $\sim 10^4$  PFU/mL) were administered directly into the placenta using the ultrasound-guided backscatter system (Visual Sonics Vevo 3100LT) as we have described.<sup>45</sup> (2) Ultrasound-guided in utero injection: Amniotic fluids embryos were directly injected with mCMV ( $10^3$  PFU in 270 nanoliter volume/embryo) using the ultrasound-guided backscatter system (Visual Sonics Vevo 3100LT) of e17.5 days' time-pregnant dams as described previously.<sup>46</sup> (3) Intraperitoneal injections in pregnant dams: Time-pregnant dams (embryonic day, e17.5) were injected with mCMV ( $10^4$  PFU/mice). (4) Intraperitoneal injections in newborn mice: Newborn pups (within 12–24 hours postbirth) were given intraperitoneal injections of mCMV ( $10^3$  PFU/mice). In all cases, CMV infection was confirmed on postnatal days 7–12 using Immediate early gene (*Ie1*) mCMV-specific primers sequence<sup>47</sup> listed in Table 1 and immunostaining of ileal tissues.

### Experimental NEC in Mice

Experimental NEC was induced in  $\sim 7$ -day-old (3- to 3.5-g body weight) mice as we have previously described and validated,<sup>48</sup> by gavage feeding (40  $\mu$ L/g body weight, 5

times daily from 7:00 AM to 7:00 PM) infant formula (Abbott Nutrition): Esbilac (PetAg) canine milk replacer, in a 2:1 ratio, which was supplemented 5 times per day with enteric bacteria obtained from a stool specimen obtained from an infant with surgical NEC. In addition, the mice were subjected to intermittent hypoxia (5% O<sub>2</sub>–95% N<sub>2</sub>, 10 minutes, twice daily) in a hypoxia chamber (Billups-Rothenberg). Age-matched breastmilk-fed pups were used as healthy control animals. Evaluation of ileal histology and expression of proinflammatory cytokines by qRT-PCR at a fixed point in the terminal ileal 2 cm proximal to the cecum was used to determine the disease severity.

### In Vivo LPS Endotoxemia and NECA Treatments in Mice

Endotoxemia was induced in control, and mCMV-infected 7- to 10-day-old neonatal mice by administering LPS (5 mg/kg, intraperitoneally, 6 hours), and distal small intestine tissues were harvested for total RNA isolation and immunohistochemical analysis. The adenosine receptor agonist NECA (0.25 mg/kg/day) was administered by oral gavage as a cotreatment with each feed on each day of the 4-day model.

### Cell and Organoid Culture

Primary intestinal crypt cultures (enteroids) were generated from the ilea of neonatal (p7–p11) C57Bl/6 mice and maintained in Matrigel (Corning). Enteroids were digested and passed using TrypLE Express (Gibco) weekly and used between passages 3 and 10 for all experiments. Mice samples were then infected with mCMV ( $5 \times 10^5$  PFU/mL) for 24–48 hours before their respective experiments. The small IEC-6 was obtained from ATCC (Manassas, VA) and maintained in culture in a growth medium consisting of Dulbecco's modified Eagle medium (Gibco BRL) supplemented with 10% fetal bovine serum (Atlanta Biosciences) and 4  $\mu$ g/mL insulin (insulin, human recombinant, zinc solution, Gibco Cat. No. 12585014) in a humidified incubator maintained at 37°C, 5% CO<sub>2</sub>. For experimental treatments, IEC-6 cells were cultured overnight in 12-well plates with or without coverslips (70%–80% confluent), infected with murine-CMV ( $5 \times 10^5$  PFU/mL) for 24–48 hours, and treated with LPS (50 mg/mL) and/or NECA (30 minutes before LPS treatment, 1  $\mu$ g/mL). For the evaluation of proinflammatory cytokine expression, cells were treated for an additional 6 hours, RNA was isolated, and qPCR was performed. For evaluation of NF- $\kappa$ B translocation from the cytoplasm to the nucleus (as a readout of LPS-TLR4 signaling), IEC-6 cells that had been infected with mCMV for 24 hours were treated with LPS (50  $\mu$ g/mL) for 45 minutes, washed in cold phosphate-buffered saline, fixed for 10 minutes with 4% fresh paraformaldehyde, blocked with 5% goat serum/0.5% bovine serum albumin, then immunostained using anti-NF- $\kappa$ B p65 subunit antibody, and examined by confocal microscopy. Nuclear NF- $\kappa$ B p65 staining was then quantified using ImageJ software as described previously.<sup>49</sup> In brief, a threshold limit was set to optimize the signal-noise ratio, and a corresponding nuclear region was defined by stenciling a circular region around DAPI-stained nuclei using the

wand tracing tool to automatically draw the nuclear area of interest. Then, nucleus-marked areas were used for NF- $\kappa$ B intensity quantification. The average integrated pixel density pertaining to the corresponding NF- $\kappa$ B p65 staining within the nuclear regions was then determined for more than 200 cells per treatment group in at least 3 replicates. Data were plotted on a scatter graph depicting the values of each individual cell, and statistical analysis was performed using Prism 10 software.

### *Histology, Immunohistochemistry, and Electron Microscopy*

**Light and Confocal Microscopy.** Freshly harvested intestinal tissues were fixed overnight with 4% paraformaldehyde and processed for paraffin embedding. Subsequently, 5  $\mu$ m tissue sections were cut from paraffin blocks using a CUT 6062 microtome (SLEE Medical GmbH, D-55129 Mainz, Germany), overnight air-dried, deparaffinized, and rehydrated for H&E and immunohistochemical staining. Samples were heated in citric acid buffer (10 mM) for antigen retrieval (pH 6, 6 minutes, 30% power in a Samsung 1200-W microwave). Sections were permeabilized with 0.1% Tween 20, blocked with 5% bovine serum albumin for nonspecific binding, probed with primary antibodies overnight at 4°C, washed, probed with secondary antibody containing DAPI (Herscht) solution for 1 hour at room temperature, and mounted using Gelvatol mount medium. After air-drying, samples were imaged using a Nikon Eclipse Ti microscope confocal laser microscope system (Nikon Instruments Inc). Confocal images were processed using ImageJ software for fluorescent intensity quantification or quantification of cells.

**Electron Microscopy.** Freshly harvested tissues were fixed in 2.5% glutaraldehyde (0.1M cacodylate buffer, pH 7.4, 4°C, 2 hours), rinsed 3 times in cacodylate buffer, postfixed in 1% osmium tetroxide buffer for 1 hour at room temperature, processed through series of dehydration steps (50%, 70%, 90%, and 100%), followed by a transition to propylene oxide as an intermediate step before infiltration, embedded in epoxy resin, and polymerized (60°C, 48 hours) to form a block suitable for sectioning. Ultrathin sections (~70 nm) were cut using an ultramicrotome equipped with a diamond knife, sections were collected on copper grids, stained with uranyl acetate and lead citrate, and imaged using a transmission electron microscope operated at an accelerating voltage optimized for high-resolution imaging of cellular and subcellular structures. Images were captured at magnifications ranging from x5000 to x30,000 to examine the ultrastructural details of the mitochondria.

### *NEC Severity Assessment*

A comprehensive, objective NEC Injury Score was developed to quantify NEC severity in mice and humans, that encompasses the key features of NEC injury, and which integrates the following:

1. Clinical findings seen in mice at necropsy: 0 = normal; 1 = minimal pneumatosis and abdominal dilation, no diarrhea or vomiting; 2 = significant pneumatosis and abdominal dilation, diarrhea, moderate weight loss; 3 = severe pneumatosis and abdominal dilation, diarrhea and bloody stools, and significant weight loss.
2. H&E staining: 0 = no injury; 1 = minor-submucosal, lamina propria separation; 2 = moderate separation of the submucosa, lamina propria, and edema in submucosal and muscular layers; 3 = severe separation of the submucosa, lamina propria, severe edema, and villous sloughing or loss of villi.
3. Proinflammatory cytokines: 0 = no changes; 1 = 25%–50% increase; 2 = 50%–75% increase; 3 = >75% increase versus unperturbed control animals.
4. Fluorescent intensity analysis of ileal 3'-NT and/or DHE immunostaining: 0 = no changes; 1 = <1-fold increase; 2 = 1.5–2.0 fold increase; 3 = >2-fold increase versus unperturbed control animals.

For human specimens, the NEC injury score is calculated on the basis of histologic damage, proinflammatory cytokines increase, and 3'-NT staining, using similar scales to mice, but a maximum score of 9, because clinical information was not available.

### *Quantitative Real-Time PCR*

Total RNA was isolated using the RNeasy Mini Kit (Qiagen), and complementary DNA was synthesized from 0.5  $\mu$ g of total RNA using the QuantiTect Reverse Transcription Kit (Qiagen) following the manufacturer's instructions. qRT-PCR was performed on the Bio-Rad CFX96 Real-Time System with iTaq Universal SYBR Green Mix (Bio-Rad) using gene-specific primers, which were designed using National Center for Biotechnology Information Primer-BLAST online program and ordered from Integrated DNA Technologies as listed in Table 1. The mRNA expression relative to the housekeeping gene ribosomal protein large P0 (Rplp0) was calculated using the  $2^{-\Delta\Delta C_t}$  method as described.<sup>50</sup>

### *Mitochondria DNA Damage and Methylation Studies*

Genomic DNA was isolated from control and NEC ileal tissues using the QIAmp DNA kit. For mtDNA damage assessments, an Optimized mtDNA qPCR primer set along with Sybr Green master mix reagents using a CFX96 Touch Real-Time PCR Detection System (Bio-Rad) were used.<sup>51</sup> The short amplicon primer pairs were used to normalize the mtDNA input, and long primer pairs were used to detect the mitochondrial lesions. The number of mtDNA lesions was calculated per 10 kb of mtDNA using an equation as previously described<sup>52</sup>: mitochondrial nicks per 10 kb =  $(1 - 2^{-(\Delta_{\text{long}} - \Delta_{\text{short}})}) \times 10 \text{ kb/fragment length per bp}$ . For methylation studies, methylation-specific PCRs were performed using forward and reverse methylation-specific primer pairs (Table 1) designed using the Meth primer design online program, <http://www.urogene.org/cgi-bin/methprimer/methprimer.cgi> and <http://www.urogene.org/cgi-bin/methprimer/methprimer.cgi>, using CpG island prediction for primer selection.

## Statistics

All data were analyzed using GraphPad Prism 10 (GraphPad Software). Data were analyzed for statistical significance by ordinary 1-way analysis of variance followed by Tukey multiple comparison test. A 2-tailed unpaired t-test with Welch comparison was used to compare data from experiments involving 2 treatment groups. A *P* value of less than 0.05 (95% confidence interval) was considered statistically significant, and data are presented as means  $\pm$  standard error of the mean. All experiments were performed with at least 3 biologic replicates and at least 3 animals per group. Graphs show individual animals as dots for each mouse specimen.

## References

- Hackam DJ, Sodhi CP. Bench to bedside: new insights into the pathogenesis of necrotizing enterocolitis. *Nat Rev Gastroenterol Hepatol* 2022;19:468–479.
- Markel TA, Martin CA, Chaaban H, et al. New directions in necrotizing enterocolitis with early-stage investigators. *Pediatr Res* 2020;88:35–40.
- Zozaya C, García González I, Avila-Alvarez A, et al. Incidence, treatment, and outcome trends of necrotizing enterocolitis in preterm infants: a multicenter cohort study. *Front Pediatr* 2020;8:188.
- Bethell GS, Knight M, Hall NJ, et al. Surgical necrotizing enterocolitis: association between surgical indication, timing, and outcomes. *J Pediatr Surg* 2021;56:1785–1790.
- Snyder KB, Calkins CL, Golubkova A, et al. Despite recovery from necrotizing enterocolitis infants retain a hyperinflammatory response to injury. *J Inflamm Res* 2024;17:331–341.
- Duess JW, Sampah ME, Lopez CM, et al. Necrotizing enterocolitis, gut microbes, and sepsis. *Gut Microbes* 2023;15:2221470.
- Warner BB, Deych E, Zhou Y, et al. Gut bacteria dysbiosis and necrotizing enterocolitis in very low birth-weight infants: a prospective case-control study. *Lancet* 2016;387:1928–1936.
- Leaphart CL, Cavallo JC, Gribar SC, et al. A critical role for TLR4 in the pathogenesis of necrotizing enterocolitis by modulating intestinal injury and repair. *J Immunol* 2007;179:4808–4820.
- Zhou Y, Li Y, Zhou B, et al. Inflammation and apoptosis: dual mediator role for toll-like receptor 4 in the development of necrotizing enterocolitis. *Inflamm Bowel Dis* 2017;23:44–56.
- Werts AD, Fulton WB, Ladd MR, et al. A novel role for necroptosis in the pathogenesis of necrotizing enterocolitis. *Cell Mol Gastroenterol Hepatol* 2020;9:403–423.
- Huang D, Wang P, Chen J, et al. Selective targeting of MD2 attenuates intestinal inflammation and prevents neonatal necrotizing enterocolitis by suppressing TLR4 signaling. *Front Immunol* 2022;13:995791.
- Scheese DJ, Sodhi CP, Hackam DJ. New insights into the pathogenesis of necrotizing enterocolitis and the dawn of potential therapeutics. *Semin Pediatr Surg* 2023;32:151309.
- Sampath V, Martinez M, Caplan M, et al. Necrotizing enterocolitis in premature infants—A defect in the brakes? Evidence from clinical and animal studies. *Mucosal Immunol* 2023;16:208–220.
- Lanzieri TM, Dollard SC, Bialek SR, et al. Systematic review of the birth prevalence of congenital cytomegalovirus infection in developing countries. *Int J Infect Dis* 2014;22:44–48.
- Shahar-Nissan K, Pardo J, Peled O, et al. Valaciclovir to prevent vertical transmission of cytomegalovirus after maternal primary infection during pregnancy: a randomised, double-blind, placebo-controlled trial. *Lancet* 2020;396:779–785.
- Coppola T, Mangold JF, Cantrell S, et al. Impact of maternal immunity on congenital cytomegalovirus birth prevalence and infant outcomes: a systematic review. *Vaccines (Basel)* 2019;7:129.
- Swanson EC, Schleiss MR. Congenital cytomegalovirus infection: new prospects for prevention and therapy. *Pediatr Clin North Am* 2013;60:335–349.
- Kenneson A, Cannon MJ. Review and meta-analysis of the epidemiology of congenital cytomegalovirus (CMV) infection. *Rev Med Virol* 2007;17:253–276.
- Zammarchi L, Tomasoni LR, Liuzzi G, et al. Treatment with valacyclovir during pregnancy for prevention of congenital cytomegalovirus infection: a real-life multicenter Italian observational study. *Am J Obstet Gynecol MFM* 2023;5:101101.
- Brizic I, Lisnic B, Brune W, et al. Cytomegalovirus infection: mouse model. *Curr Protoc Immunol* 2018;122:e51.
- Gamadia LE, Remmerswaal EB, Weel JF, et al. Primary immune responses to human CMV: a critical role for IFN- $\gamma$ -producing CD4 $^{+}$  T cells in protection against CMV disease. *Blood* 2003;101:2686–2692.
- Knoblauch T, Grandel B, Seiler J, et al. Human cytomegalovirus IE1 protein elicits a type II interferon-like host cell response that depends on activated STAT1 but not interferon- $\gamma$ . *PLoS Pathog* 2011;7:e1002016.
- Saha B, Jyothi Prasanna S, et al. Gene modulation and immunoregulatory roles of interferon gamma. *Cytokine* 2010;50:1–14.
- Sodhi CP, Neal MD, Siggers R, et al. Intestinal epithelial Toll-like receptor 4 regulates goblet cell development and is required for necrotizing enterocolitis in mice. *Gastroenterology* 2012;143:708–718.e5.
- Esteki-Zadeh A, Karimi M, Straat K, et al. Human cytomegalovirus infection is sensitive to the host cell DNA methylation state and alters global DNA methylation capacity. *Epigenetics* 2012;7:585–593.
- Combs JA, Norton EB, Saifudeen ZR, et al. Human cytomegalovirus alters host cell mitochondrial function during acute infection. *J Virol* 2020;94:e01183–19.
- Huang C, Deng K, Wu M. Mitochondrial cristae in health and disease. *Int J Biol Macromol* 2023;235:123755.
- Jezek P, Jaburek M, Holendova B, et al. Mitochondrial cristae morphology reflecting metabolism, superoxide formation, redox homeostasis, and pathology. *Antioxid Redox Signal* 2023;39:635–683.
- Lee SJ, Zhang J, Choi AM, et al. Mitochondrial dysfunction induces formation of lipid droplets as a generalized response to stress. *Oxid Med Cell Longev* 2013;2013:327167.



30. Bachman LO, Zvezdaryk KJ. Targeting the host mitochondria as a novel human cytomegalovirus Antiviral Strategy. *Viruses* 2023;15:1083.
31. Monk CH, Zvezdaryk KJ. Host mitochondrial requirements of cytomegalovirus replication. *Curr Clin Microbiol Rep* 2020;7:115–123.
32. Tyl MD, Betsinger CN, Cristea IM. Virus-host protein interactions as footprints of human cytomegalovirus replication. *Curr Opin Virol* 2022;52:135–147.
33. Sodhi CP, Fulton WB, Good M, et al. Fat composition in infant formula contributes to the severity of necrotizing enterocolitis. *Br J Nutr* 2018;120:665–680.
34. Sodhi CP, Gonzalez Salazar AJ, Kovler ML, et al. The administration of a pre-digested fat-enriched formula prevents necrotizing enterocolitis-induced lung injury in mice. *Br J Nutr* 2022;128:1050–1063.
35. Zhang L, Fan J, He J, et al. Regulation of ROS-NF- $\kappa$ B axis by tuna backbone derived peptide ameliorates inflammation in necrotizing enterocolitis. *J Cell Physiol* 2019;234:14330–14338.
36. Aydemir C, Dilli D, Uras N, et al. Total oxidant status and oxidative stress are increased in infants with necrotizing enterocolitis. *J Pediatr Surg* 2011;46:2096–2100.
37. Tan JBC, Boskovic DS, Angeles DM. The energy costs of prematurity and the neonatal intensive care unit (NICU) experience. *Antioxidants (Basel)* 2018;7:37.
38. Kong X, Thimmulappa R, Kombairaju P, et al. NADPH oxidase-dependent reactive oxygen species mediate amplified TLR4 signaling and sepsis-induced mortality in Nrf2-deficient mice. *J Immunol* 2010;185:569–577.
39. Omarsdottir S, Agnarsdottir M, Casper C, et al. High prevalence of cytomegalovirus infection in surgical intestinal specimens from infants with necrotizing enterocolitis and spontaneous intestinal perforation: a retrospective observational study. *J Clin Virol* 2017;93:57–64.
40. Neuberger P, Hamprecht K, Vochem M, et al. Case-control study of symptoms and neonatal outcome of human milk-transmitted cytomegalovirus infection in premature infants. *J Pediatr* 2006;148:326–331.
41. Skeath T, Stewart C, Waugh S, et al. Cytomegalovirus and other common enteric viruses are not commonly associated with NEC. *Acta Paediatr* 2016;105:50–52.
42. Mani S, Hazra S, Hagan J, et al. Viral infections and neonatal necrotizing enterocolitis: a meta-analysis. *Pediatrics* 2023;152:e2022060876.
43. Teresa C, Antonella D, de Ville de Goyet J. New nutritional and therapeutical strategies of NEC. *Curr Pediatr Rev* 2019;15:92–105.
44. Afrazi A, Branca MF, Sodhi CP, et al. Toll-like receptor 4-mediated endoplasmic reticulum stress in intestinal crypts induces necrotizing enterocolitis. *J Biol Chem* 2014;289:9584–9599.
45. Takahashi K, Endo M, Miyoshi T, et al. Immune tolerance induction using fetal directed placental injection in rodent models: a murine model. *PLoS One* 2015;10:e0123712.
46. Gribar SC, Sodhi CP, Richardson WM, et al. Reciprocal expression and signaling of TLR4 and TLR9 in the pathogenesis and treatment of necrotizing enterocolitis. *J Immunol* 2009;182:636–646.
47. Kamimura Y, Lanier LL. Rapid and sequential quantitation of salivary gland-associated mouse cytomegalovirus in oral lavage. *J Virol Methods* 2014;205:53–56.
48. Kovler ML, Sodhi CP, Hackam DJ. Precision-based modeling approaches for necrotizing enterocolitis. *Dis Model Mech* 2020;13:dmm044388.
49. Sodhi CP, Ahmad R, Jia H, et al. The administration of amnion-derived multipotent cell secretome ST266 protects against necrotizing enterocolitis in mice and piglets. *Am J Physiol Gastrointest Liver Physiol* 2022;323:G265–G282.
50. Livak KJ, Schmittgen TD. Analysis of relative gene expression data using real-time quantitative PCR and the 2(-Delta Schmittgen C(T)) method. *Methods* 2001;25:402–408.
51. Gureev AP, Shaforostova EA, Starkov AA, et al. Simplified qPCR method for detecting excessive mtDNA damage induced by exogenous factors. *Toxicology* 2017;382:67–74.
52. Rothfuss O, Gasser T, Patenge N. Analysis of differential DNA damage in the mitochondrial genome employing a semi-long run real-time PCR approach. *Nucleic Acids Res* 2010;38:e24.

---

Received September 29, 2024. Accepted January 27, 2025.

#### Correspondence

Address correspondence to: David J. Hackam, MD, PhD, Division of Pediatric Surgery, Johns Hopkins University, Room 7323, 1800 Orleans Street, Baltimore, Maryland 21287. e-mail: [Dhackam1@jhmi.edu](mailto:Dhackam1@jhmi.edu); or Chhinder P. Sodhi, PhD, Division of Pediatric Surgery, Johns Hopkins University, Room 7323, 1800 Orleans Street, Baltimore, Maryland 21287. e-mail: [csodhi@jhmi.edu](mailto:csodhi@jhmi.edu).

#### Acknowledgements

Daniel Scheese, Peng Lu, and Chhinder P. Sodhi contributed equally to this work.

#### CRedit Authorship Contributions

Daniel Scheese, MD (Conceptualization: Equal; Investigation: Lead; Writing – original draft: Lead; Writing – review & editing: Equal)  
 Peng Lu, PhD (Conceptualization: Equal; Investigation: Equal; Methodology: Equal)  
 Hannah Moore (Formal analysis: Equal; Investigation: Supporting; Writing – original draft: Supporting)  
 Koichi Tsuboi, MD (Investigation: Supporting)  
 Cody Tragesser, MD (Investigation: Supporting)  
 Johannes Dues, PhD, MD (Investigation: Supporting)  
 Zachariah Raouf, MD (Investigation: Supporting)  
 Maame Sampah, PhD, MD (Investigation: Supporting)  
 Daphne Klerk (Investigation: Supporting)  
 Mahmoud El Baassiri, MD (Investigation: Supporting)  
 Hee-Seong Jang, PhD (Investigation: Supporting)  
 Sierra Williams-McLeod (Investigation: Supporting)  
 Asuka Ishiyama, MD (Investigation: Supporting)  
 Steve Steinway, PhD, MD (Investigation: Supporting)  
 Sanxia Wang (Investigation: Supporting)  
 Menghan Wang (Investigation: Supporting)  
 Thomas Prindle (Investigation: Supporting)  
 William Fulton, MS (Conceptualization: Supporting; Investigation: Supporting; Supervision: Equal)  
 Chhinder Sodhi, PhD (Conceptualization: Equal; Formal analysis: Lead; Investigation: Equal; Supervision: Equal; Visualization: Equal; Writing – original draft: Equal; Writing – review & editing: Equal)  
 David J. Hackam, PhD, MD (Conceptualization: Lead; Funding acquisition: Lead; Project administration: Lead; Supervision: Lead; Writing – original draft: Equal; Writing – review & editing: Equal)

#### Conflicts of interest

The authors disclose no conflicts.

#### Funding

David J. Hackam is funded by NIH R35 GM141956. Daniel Scheese and Cody Tragesser are funded by NIH T32 DK007713. David J. Hackam is also supported by the Garrett Fund for the Surgical Treatment of Children, at the Johns Hopkins University.